J. Fluid Mech. (1991), *vol.* 222, *pp.* 471–499
Printed in Great Britain

Standing radial cross-waves†

By JANET M. BECKER‡ AND JOHN W. MILES
Institute of Geophysics and Planetary Physics, University of California, San Diego, La Jolla, CA 92093, USA

(Received 14 November 1989 and in revised form 13 June 1990)

Standing radial cross-waves in an annular wave tank are investigated using Whitham's average-Lagrangian method. For the simplest case, in which a single radial cross-wave is excited, energy is transferred from the wavemaker to the cross-wave through the spatial mean motion of the free surface, as described by Garrett (1970) for a purely transverse cross-wave in a rectangular tank. In addition, energy is transferred through spatial coupling since, in contrast to the purely transverse cross-wave in the rectangular tank, the (non-axisymmetric) radial cross-wave is three-dimensional. It is shown in an Appendix that this spatial coupling does occur for a three-dimensional cross-wave in a rectangular tank. The equations that govern this single-mode resonance are isomorphic to those that govern the Faraday resonance of surface waves in a basin of fluid subjected to vertical excitation (Miles 1984*a*).

It is found that the second-order Stokes-wave expansion for deep-water, standing gravity waves, which is regular for rectangular containers, may become singular for circular containers (Mack (1962) noted these resonances for finite-depth, standing gravity waves in circular containers). The evolution equations that govern two distinct types of resonant behaviour are derived: (i) 2:1 resonance between a radial cross-wave and a resonantly forces axisymmetric wave, corresponding to approximate equality among the driving frequency, a natural frequency of the directly forced wave, and twice the natural frequency of a cross-wave; (ii) 2:1 internal resonance between a radial cross-wave and a non-axisymmetric second harmonic, corresponding to approximate equality among the driving frequency, the natural frequency of a non-axisymmetric wave of even azimuthal wavenumber, and twice the natural frequency of the cross-wave. The axisymmetric, directly forced wave in (i) is resonantly excited and exchanges energy with the subharmonic cross-wave through spatial coupling, whereas the cross-wave in (ii) is parametrically excited and exchanges energy with the non-axisymmetric second harmonic through spatial coupling. The equations governing case (i) are shown to exhibit chaotic motions; those governing (ii) are shown to be isomorphic to the equations governing 2:1 internal resonance in the Faraday problem (Miles 1984*a*, §6), which have been shown to exhibit chaotic motions (Gu & Sethna 1987).

Preliminary experiments on standing radial cross-waves are reported in an Appendix, and theoretical predictions of mode stability are in qualitative agreement with these experiments. For the single-mode theory, the interaction coefficient that is a measure of the energy exchange between the wavemaker and the cross-wave is evaluated numerically for a particular wavemaker. The maximum interaction

† With an Appendix by Janet M. Becker and Diane M. Henderson.

‡ Present address: School of Mathematics, The University of New South Wales, Kensington, NSW 2033, Australia.

coefficient for a fixed azimuthal wavenumber of the cross-wave typically occurs for that radial mode number for which the turning point of the cross-wave radial profile is nearest the wavemaker. The present experiments for standing radial cross-waves are compared with those of Tatsuno, Inoue & Okabe (1969) for progressive radial cross-waves.

1. Introduction

We consider here standing, radial cross-waves in an annular wave tank. Cross-waves emanate from a symmetry-breaking instability that may occur when surface waves of finite amplitude are excited by a wavemaker. They have crests perpendicular to, and frequency half that of, the wavemaker. In 1831 Faraday (see Martin 1932) observed the excitation of cross-waves by a vibrating plate and of radial cross-waves by a vibrating cork (see Miles & Henderson (1990) for a discussion). A symmetric (independent of the cross-channel coordinate) wavemaker oscillating in a rectangular wave tank is related to Faraday's vibrating-plate experiment. Garrett (1970), Miles (1988, hereinafter referred to as I) and Tsai, Yue & Yip (1990) have studied the excitation of a purely transverse cross-wave by a symmetric wavemaker in a short (length $\approx$ breadth) rectangular tank. The more difficult problem of progressive cross-waves in a long (length $\gg$ breadth) rectangular tank has been studied by Mahony (1972), Jones (1984), Lichter & Chen (1987) and Miles & Becker (1988). Radial cross-waves in an annular wave tank, which are related to Faraday's vibrating-cork experiment, do not appear to have been previously studied.

We examine the excitation of gravity waves of free-surface displacement ζ in an annular wave tank of inner radius r_1, outer radius r_2 and depth d by the wavemaker displacement

$$r = r_1 + \chi = r_1 + af(z)\sin 2\omega t \quad (0 < \theta < 2\pi, \quad -d < z < \zeta), \tag{1.1}$$

on the assumptions that

$$k_{\nu m} a \equiv \epsilon \ll 1, \quad k_{\nu m} d \gg 1, \quad k_{\nu m}(r_2 - r_1) = O(1), \tag{1.2a–c}$$

where $k_{\nu m}$ is the wavenumber of the radial cross-wave defined by

$$J'_\nu(k_{\nu m} r_2)\, Y'_\nu(k_{\nu m} r_1) - J'_\nu(k_{\nu m} r_1)\, Y'_\nu(k_{\nu m} r_2) = 0 \quad (\nu = 1, 2, \ldots, m = 0, 1, 2, \ldots), \tag{1.3a}$$

and J_ν/Y_ν are Bessel functions of order ν of the first/second kind. An axisymmetric wave is directly forced by the wavemaker. In addition, when ω approximates a natural frequency of a radial cross-wave,

$$\omega_{\nu m} = (g k_{\nu m})^{\frac{1}{2}}, \tag{1.3b}$$

nonlinear coupling may transfer energy from the wavemaker to the cross-wave. We first assume that ω approximates $\omega_{\nu m}$ according to

$$\frac{\omega^2 - \omega_{\nu m}^2}{\omega^2} = 1 - \frac{k_{\nu m}}{\kappa} = O(\epsilon) \quad \left(\kappa \equiv \frac{\omega^2}{g}\right), \tag{1.4}$$

which fixes the bandwidth of the resonance.

We pose the free surface displacement of the radial cross-wave in the form

$$\zeta = \epsilon^{-\frac{1}{2}} a \,\mathrm{Re}\,[(p+\mathrm{i}q)\,\mathrm{e}^{-\mathrm{i}\omega t}]\frac{J_\nu(k_{\nu m}\,r)\,Y'_\nu(k_{\nu m}\,r_1)-J'_\nu(k_{\nu m}\,r_1)\,Y_\nu(k_{\nu m}\,r)}{N_\nu}\cos\nu\theta, \qquad (1.5)$$

where $p+\mathrm{i}q$ is a dimensionless, slowly varying, complex amplitude and N_ν is a normalization coefficient. We then use Whitham's average-Lagrangian method to obtain the evolution equations that govern (p, q). These equations are isomorphic to those in I §5.

Radial cross-waves resemble cross-waves in a rectangular wave tank, but there are significant differences. The first difference may be elucidated by considering how energy is transferred from the wavemaker to the cross-wave. As noted by Garrett (1970), the dominant mechanism by which energy is transferred from a symmetric wavemaker to a purely transverse (two-dimensional) cross-wave in a rectangular tank is through coupling between the cross-wave and the spatially averaged motion of the directly forced wave. For a radial cross-wave, which is inherently three-dimensional, energy also is transferred through spatial coupling, which may be represented by an infinite sum over the axisymmetric free modes (of zero spatial mean) in the annulus. This spatial coupling, which is absent for a two-dimensional cross-wave, does occur for a three-dimensional cross-wave in a rectangular tank (see Appendix A).

The second difference between cross-waves in a rectangular wave tank and radial cross-waves is elucidated by considering the second-order Stokes-wave expansion for deep-water, standing gravity waves, which is regular for rectangular containers but may become singular for circular containers.† Hunt & Baddour (1980) have carried out this Stokes-wave expansion to second order for deep-water, standing gravity waves in a circular cylinder or annulus. We find that small divisors occur in their expansion, in consequence of which their ordering breaks down and resonances may occur.

Internal resonance between a radial cross-wave and an axisymmetric second harmonic corresponds to approximate equality among the driving frequency, a natural frequency of the directly forced wave, and twice the natural frequency of the cross-wave. We derive the equations that govern this resonance and find that chaotic motions occur in some parametric domains. Since 2:1 internal resonance cannot occur for cross-waves in a rectangular wave tank, the corresponding equations must have higher-order nonlinearity than those for radial cross-waves, for which the nonlinearity is quadratic. We also consider internal resonance between a radial cross-wave and a non-axisymmetric second harmonic, for which the governing equations are isomorphic to those in Miles (1984*a*, §6) and have been shown to admit chaotic solutions (Gu & Sethna 1987).

We begin our analysis, in §2, with the variational formulation for standing radial cross-waves in an annulus. We present the trial functions in §3. Here, in contrast to I, we develop an explicit representation for the directly forced wave rather than considering only its mean properties (see Appendix B). In §4, we obtain the average Lagrangian, and in §5 we obtain the evolution equations and quote the results of I §5 for the stability analysis. In §6, we consider the case when the driving frequency approximates both a natural frequency of the directly forced wave and twice that of the cross-wave. In §7, we consider the case when the driving frequency approximates

† These internal resonances were recognized by Mack (1962) for finite-depth, standing gravity waves in circular containers.

both the natural frequency of a non-axisymmetric wave of even azimuthal wavenumber and twice that of the cross-wave. We consider three-dimensional cross-waves in a rectangular wave tank in Appendix A.

Two-dimensional cross-waves in a rectangular wave tank have been examined experimentally by Lin & Howard (1960). Garrett (1970) and Tsai *et al.* (1990) have shown agreement between the theoretical predictions of the frequency–amplitude relationship for the cross-waves and Lin & Howard's data. Preliminary experimental results on standing radial cross-waves are presented in Appendix C; our theoretical predictions of mode stability are in qualitative agreement with these data. The interaction coefficient that is a measure of the energy exchange between the wavemaker and the cross-wave is evaluated numerically in Appendix C for a particular wavemaker. For a fixed azimuthal wavenumber, ν, the maximum energy-exchange coefficient typically occurs for that mode for which $k_{\nu m} \approx \nu/r_1$. We conclude by comparing the present experimental data for standing radial cross-waves with those of Tatsuno, Inoue & Okabe (1969) for progressive radial cross-waves. A theoretical analysis for progressive radial cross-waves is currently being developed.

2. Variational formulation

The boundary-value problem that governs the velocity potential $\phi(r,\theta,z,t)$ and the free-surface displacement $\zeta(r,\theta,t)$, for motion started from rest in an inviscid, incompressible fluid confined to the annular wave tank described in §1 is

$$\nabla^2\phi = 0 \quad (r_1+\chi < r < r_2, \quad 0 < \theta < 2\pi, \quad -d < z < \zeta), \tag{2.1}$$

$$\phi_z = \zeta_t + \nabla\phi\cdot\nabla\zeta, \quad \phi_t + \tfrac{1}{2}(\nabla\phi)^2 + g\zeta = 0 \quad (z=\zeta), \tag{2.2a, b}$$

$$\phi_r = 0 \quad (r=r_2), \quad \phi_\theta|_{\theta=0} = \phi_\theta|_{\theta=2\pi}, \quad \phi_z = 0 \quad (z=-d), \tag{2.3a–c}$$

$$\phi_r = \chi_t + \nabla\phi\cdot\nabla\chi \quad (r=r_1+\chi), \tag{2.4}$$

where the subscripts r,θ,z,t signify partial differentiation. The boundary condition (2.3*c*) is imposed at $z=-\infty$ (deep-water waves) in §§3–7.

Equations (2.1)–(2.4) may be deduced from the variational principle

$$\delta J = 0, \quad J \equiv \int \hat{L}\,\mathrm{d}t, \tag{2.5a, b}$$

where J is the action integral of the Lagrangian (Luke 1967; Miloh 1984; I §2),

$$\hat{L} = -\iiint [\phi_t + \tfrac{1}{2}(\nabla\phi)^2 + gz]\,\mathrm{d}V, \tag{2.6}$$

and the volume integral is over the domain bounded by the wavemaker ($r = r_1+\chi$), the free surface ($z=\zeta$), and the fixed boundaries ($r=r_2$, $\theta = 0, 2\pi$, and $z=-d$). Following I §2, we transform (2.6) to

$$L = \frac{1}{2}\int_0^{2\pi}\mathrm{d}\theta\left\{\iint\phi\nabla^2\phi r\,\mathrm{d}r\,\mathrm{d}z + \int_{r_0}^{r_2}[\phi(2\zeta_t-\phi_z+\nabla\phi\cdot\nabla\zeta)-g\zeta^2]_{z=\zeta} r\,\mathrm{d}r\right.$$
$$\left.\int_{-d}^{z_0}[r\phi(\phi_r-\nabla\chi\cdot\nabla\phi-2\chi_t)-grz^2\chi_z]_{r=r_1+\chi}\mathrm{d}z\right\}, \tag{2.7}$$

where $r_0(\theta,t)$ and $z_0(\theta,t)$ are the coordinates of the intersection of the wavemaker ($r = r_1+\chi$) with the free surface ($z = \zeta$).

3. Trial functions

We choose the trial functions

$$(k_{\nu m}\omega/g)\,\phi = \epsilon^{\frac{1}{2}}\phi_1+\epsilon(\phi_{11}+\phi_0)+O(\epsilon^{\frac{3}{2}}) \tag{3.1a}$$

and

$$k_{\nu m}\zeta = \epsilon^{\frac{1}{2}}\zeta_1+\epsilon(\zeta_{11}+\zeta_0)+O(\epsilon^{\frac{3}{2}}). \tag{3.1b}$$

Here, (ϕ_1,ζ_1), which represent the first-order cross-wave and satisfy the unforced ($\chi = 0$ in (2.4)), linear dynamics, are given by

$$\phi_1 = \mathrm{Re}\,[\{q(\tau)-\mathrm{i}p(\tau)\}\,\mathrm{e}^{-\mathrm{i}\omega t}]\,F_\nu(\rho)\cos\nu\theta\,\mathrm{e}^{\xi}, \tag{3.2a}$$

$$\zeta_1 = \mathrm{Re}\,[\{p(\tau)+\mathrm{i}q(\tau)\}\,\mathrm{e}^{-\mathrm{i}\omega t}]\,F_\nu(\rho)\cos\nu\theta, \tag{3.2b}$$

where $\nu = 1,2,\ldots$ is the azimuthal wavenumber of the radial cross-wave (which, by definition is non-axisymmetric),

$$\rho \equiv k_{\nu m}r, \quad \rho_1 \equiv k_{\nu m}r_1, \quad \rho_2 \equiv k_{\nu m}r_2, \quad \xi \equiv k_{\nu m}z \tag{3.3a–d}$$

are the dimensionless radial coordinate, inner and outer cylinder radius, and vertical coordinate,

$$\tau \equiv \epsilon\omega t, \tag{3.3e}$$

is a dimensionless slow time, and

$$F_\nu(\rho) \equiv \frac{1}{N_\nu}[J_\nu(\rho)\,Y'_\nu(\rho_1)-J'_\nu(\rho_1)\,Y_\nu(\rho)], \tag{3.4a}$$

is the radial eigenfunction for the cross-wave, with N_ν fixed by

$$\int_{\rho_1}^{\rho_2} F_\nu^2(\rho)\,\rho\,\mathrm{d}\rho = 1. \tag{3.4b}$$

(ϕ_0,ζ_0) represent the axisymmetric, directly forced wave and are defined below in (3.10).

The second-order cross-wave is given by†

$$\phi_{11} = \mathrm{Re}\,[\tfrac{1}{2}\mathrm{i}(p+\mathrm{i}q)^2\,\mathrm{e}^{-2\mathrm{i}\omega t}]\left\{A_0+\sum_{n=1}^{\infty}A_n\,F_0(\mu_n\rho)\,\mathrm{e}^{\mu_n\xi}+\cos 2\nu\theta\sum_{n=0}^{\infty}B_n\,F_{2\nu}(\gamma_n\rho)\,\mathrm{e}^{\gamma_n\xi}\right\} \tag{3.5a}$$

$$\begin{aligned}\zeta_{11} = {} & -\mathrm{Re}\,[\tfrac{1}{8}(p+\mathrm{i}q)^2\,\mathrm{e}^{-2\mathrm{i}\omega t}]\left\{\sum_{n=1}^{\infty}2\mu_n A_n\,F_0(\mu_n\rho)+\frac{1}{\rho}[\rho F_\nu(\rho)\,F'_\nu(\rho)]'\right.\\ & \left.+\cos 2\nu\theta\left[\sum_{n=0}^{\infty}2\gamma_n B_n\,F_{2\nu}(\gamma_n\rho)+\frac{1}{\rho}[\rho F_\nu(\rho)\,F'_\nu(\rho)]'-\frac{2\nu^2}{\rho^2}F_\nu^2(\rho)\right]\right\}\\ & -\tfrac{1}{8}(p^2+q^2)\left\{\frac{1}{\rho}[\rho F_\nu(\rho)\,F'_\nu(\rho)]'+\cos 2\nu\theta\left[\frac{1}{\rho}[\rho F_\nu(\rho)\,F'_\nu(\rho)]'-\frac{2\nu^2}{\rho^2}F_\nu^2(\rho)\right]\right\},\end{aligned} \tag{3.5b}$$

† The equivalents of (3.2), (3.5*a*) and (3.6) are given in Hunt & Baddour (1980).

where

$$A_0 \equiv \frac{1}{\rho_2^2-\rho_1^2}, \quad A_n \equiv \frac{1}{4-\mu_n}\int_{\rho_1}^{\rho_2}\rho\,\mathrm{d}\rho\,F_0(\mu_n\rho)\left[F_\nu'^2(\rho)+\left(1+\frac{\nu^2}{\rho^2}\right)F_\nu^2(\rho)\right]$$

$$= \frac{1}{2}\left[\frac{4-\mu_n^2}{4-\mu_n}\right]\int_{\rho_1}^{\rho_2}\rho\,\mathrm{d}\rho\,F_0(\mu_n\rho)\,F_\nu^2(\rho) \quad (n=1,2,\ldots), \quad (3.6a,b)$$

$$B_n \equiv \frac{1}{4-\gamma_n}\int_{\rho_1}^{\rho_2}\rho\,\mathrm{d}\rho\,F_{2\nu}(\gamma_n\rho)\left[F_\nu'^2(\rho)+\left(1-\frac{\nu^2}{\rho^2}\right)F_\nu^2(\rho)\right]$$

$$= \frac{1}{2}\left[\frac{4-\gamma_n^2}{4-\gamma_n}\right]\int_{\rho_1}^{\rho_2}\rho\,\mathrm{d}\rho\,F_{2\nu}(\gamma_n\rho)\,F_\nu^2(\rho) \quad (n=0,1,2,\ldots); \quad (3.6c)$$

$F_0(\mu_n\rho)$ and $F_{2\nu}(\gamma_n\rho)$ are the radial eigenfunctions,

$$F_0(\mu_n\rho) \equiv \frac{1}{N_0}[J_1(\mu_n\rho_1)\,Y_0(\mu_n\rho)-J_0(\mu_n\rho)\,Y_1(\mu_n\rho_1)] \quad (n=1,2,\ldots), \quad (3.7a)$$

$$F_{2\nu}(\gamma_n\rho) \equiv \frac{1}{N_{2\nu}}[J_{2\nu}(\gamma_n\rho)\,Y_{2\nu}'(\gamma_n\rho_1)-J_{2\nu}'(\gamma_n\rho_1)\,Y_{2\nu}(\gamma_n\rho)] \quad (n=0,1,2,\ldots), \quad (3.7b)$$

normalized according to

$$\int_{\rho_1}^{\rho_2}F_0^2(\mu_n\rho)\,\rho\,\mathrm{d}\rho = 1, \quad \int_{\rho_1}^{\rho_2}F_{2\nu}^2(\gamma_n\rho)\,\rho\,\mathrm{d}\rho = 1, \quad (3.8a,b)$$

and the eigenvalues, μ_n and γ_n are fixed by

$$F_0'(\mu_n\rho_2) = 0 \quad (n=1,2,\ldots), \quad F_{2\nu}'(\gamma_n\rho_2) = 0 \quad (n=0,1,2,\ldots). \quad (3.9a,b)$$

We note that $$\mu_n = k_{0n}/k_{\nu m}, \quad \gamma_n = k_{2\nu n}/k_{\nu m}. \quad (3.9c,d)$$

For the present calculation, we assume that neither μ_n nor γ_n approximate 4 (but see §§6–7).

In contrast to I, an explicit representation of the wavemaker solution (ϕ_0, ζ_0) is necessary for the evaluation of the integral over the free surface in (2.7). The modification of Havelock's (1929) solution of the wavemaker problem to accommodate standing waves is straightforward; however, it is more convenient to express the solution to the linear truncations of (2.1)–(2.4) as an infinite sum of free modes. Physically, this representation corresponds to replacing the motion of the wavemaker by an equivalent mass source located at $x = 0$. Solving (2.1)–(2.4), using the finite Hankel transform (cf. Sneddon 1972), we obtain

$$\phi_0 = \cos 2\omega t\left[\frac{2\rho_1}{\rho_2^2-\rho_1^2}\Phi_0(\xi)+\frac{2}{\pi}\sum_{n=1}^{\infty}\frac{\Phi_{\mu_n}(\xi)}{N_0\mu_n}F_0(\mu_n\rho)\right], \quad (3.10a)$$

$$\zeta_0 = 2\sin 2\omega t\left[\frac{2\rho_1}{\rho_2^2-\rho_1^2}\Phi_0(0)+\frac{2}{\pi}\sum_{n=1}^{\infty}\frac{\Phi_{\mu_n}(0)}{N_0\mu_n}F_0(\mu_n\rho)\right], \quad (3.10b)$$

where $\Phi_0(\xi)$ and the $\Phi_{\mu_n}(\xi)$, $(n=1,2,\ldots)$ are given in Appendix B. We note that the non-uniform validity of (3.10) as $r \downarrow r_1$ does not affect the following results, since (2.4) is applied directly in the integral over the wavemaker in (2.7) (see §4). We anticipate

that, in the series (3.10), only $\Phi_0(\xi)$ and $\Phi_{\mu_n}(\xi)$ and their derivatives, evaluated at the rest position of the free surface $\xi = 0$, are required:

$$\Phi_0(0) = \frac{1}{2}\int_{-\infty}^{0} f(s)\,\mathrm{d}s, \quad \Phi_0'(0) = 4\Phi_0(0), \quad \Phi_0''(0) = 2f(0), \tag{3.11a–c}$$

$$\Phi_{\mu_n}(0) = \frac{2}{4-\mu_n}\int_{-\infty}^{0} f(s)\,\mathrm{e}^{\mu_n s}\,\mathrm{d}s, \quad \Phi_{\mu_n}'(0) = 4\Phi_{\mu_n}(0), \tag{3.12a, b}$$

$$\Phi_{\mu_n}''(0) = \mu_n^2\,\Phi_{\mu_n}(0) + 2f(0), \tag{3.12c}$$

where, here and subsequently, primes indicate differentiation with respect to argument.

4. The average Lagrangian

We next substitute (3.1) into (2.7) and average over ωt to obtain the average Lagrangian $\langle L\rangle$ as a functional of p and q. Since $\nabla^2(3.1a) = 0$, the volume integral in (2.7) vanishes, and the calculation is reduced to integrals over the free surface and the wavemaker. We subdivide $\langle L\rangle$ according to

$$\langle L\rangle = \tfrac{1}{2}\langle F + W + B_{\mathrm{f}} + B_{\mathrm{w}}\rangle, \tag{4.1}$$

where

$$F \equiv \int_0^{2\pi}\int_{r_1}^{r_2} I_{\mathrm{f}}\, r\,\mathrm{d}r\,\mathrm{d}\theta, \quad W \equiv \int_0^{2\pi}\int_{-\infty}^{0} I_{\mathrm{w}}\,\mathrm{d}z\,\mathrm{d}\theta, \tag{4.2a, b}$$

are integrals over the rest positions of the free surface and the wavemaker,

$$B_{\mathrm{f}} \equiv \int_0^{2\pi}\int_{r_0}^{r_1} I_{\mathrm{f}}\, r\,\mathrm{d}r\,\mathrm{d}\theta, \quad B_{\mathrm{w}} \equiv \int_0^{2\pi}\int_{0}^{z_0} I_{\mathrm{w}}\,\mathrm{d}z\,\mathrm{d}\theta, \tag{4.3a, b}$$

are the contributions from the endpoints,

$$I_{\mathrm{f}} \equiv [\phi(2\zeta_t - \phi_z + \nabla\phi\cdot\nabla\zeta) - g\zeta^2]_{z=\zeta}, \quad I_{\mathrm{w}} \equiv [r\phi(\phi_r - \nabla\chi\cdot\nabla\phi - 2\chi_t) - grz^2\chi_z]_{r=r_1+\chi} \tag{4.4a, b}$$

are the integrands of the free surface and wavemaker integrals, and (ϕ, ζ) are given by (3.1).

We approximate the contributions from the endpoints, (4.3), by (cf. I (4.1))

$$B_{\mathrm{f}} = \int_0^{2\pi}\left\{-I_{\mathrm{f}}|_{r=r_1}(r_0 - r_1) + O\left[\left(\frac{\mathrm{d}I_{\mathrm{f}}}{\mathrm{d}r}, \frac{I_{\mathrm{f}}}{r_1}\right)\Big|_{r=r_1}(r_0 - r_1)^2\right]\right\} r_1\,\mathrm{d}\theta, \tag{4.5a}$$

$$B_{\mathrm{w}} = \int_0^{2\pi}\left\{I_{\mathrm{w}}|_{z=0}\, z_0 + O\left[\frac{\mathrm{d}I_{\mathrm{w}}}{\mathrm{d}z}\Big|_{z=0} z_0^2\right]\right\}\mathrm{d}\theta. \tag{4.5b}$$

Invoking (1.1) and (2.4), remarking that

$$r_0 = r_1 + \chi(0,t) + O(\epsilon^{\frac{3}{2}}), \quad z_0 = \zeta(r_1,\theta,t) + O(\epsilon^{\frac{3}{2}}),$$

summing, and averaging, we obtain

$$\langle B_{\mathrm{f}} + B_{\mathrm{w}}\rangle = \frac{\epsilon^2 g f(0)}{k_{\nu m}^4}\int_0^{2\pi}\langle(\zeta_1^2 - \phi_1\phi_{1\xi})\sin 2\omega t - 2\phi_1\zeta_1\cos 2\omega t\rangle\,\mathrm{d}\theta + O(\epsilon^3). \tag{4.6a}$$

Substituting (3.2) into (4.6), we find that $\langle B_{\mathrm{f}} + B_{\mathrm{w}}\rangle = O(\epsilon^3)$; hence (4.1) reduces to

$$\langle L\rangle = \tfrac{1}{2}\langle F + W\rangle + O(\epsilon^3). \tag{4.6b}$$

For the free-surface integral (4.2a), we replace $\omega^{-1}\partial_t$ by $\omega^{-1}\partial_t+\epsilon\partial_\tau$, invoke (3.2), (3.5) and (3.10), integrate, and average to obtain

$$\langle F-F_0\rangle = \frac{2\epsilon^2 g\pi}{k_{\nu m}^4}\langle F_1+F_{10}+F_{11}\rangle+O(\epsilon^3), \tag{4.7}$$

where F_0 represents that part of the free-surface integral due to the directly forced wave (and hence is independent of p and q); F_1 represents quadratic interactions of the first-order cross-wave, (3.2), that are raised $O(\epsilon^2)$ by slow modulation and resonant detuning,

$$\langle F_1\rangle = \tfrac{1}{2}(\dot{p}q-p\dot{q})+\tfrac{1}{2}\beta(p^2+q^2), \tag{4.8}$$

where, here and subsequently, the dot indicates differentiation with respect to τ, and

$$\beta \equiv \frac{\omega^2-\omega_{\nu m}^2}{2\epsilon\omega^2} = \frac{(1-(k_{\nu m}/\kappa))}{2\epsilon} \tag{4.9}$$

is a tuning parameter; F_{10} represents the interaction of the forced-wave, (3.10), with the cross-wave (3.2, 3.5),

$$\begin{aligned}\langle F_{10}\rangle &= \tfrac{1}{4}pq\left\{\frac{2\rho_1}{\rho_2^2-\rho_1^2}[\Phi_0'(0)-\Phi_0''(0)]\right.\\ &\quad\left.+\frac{2}{\pi}\sum_{n=1}^{\infty}\frac{1}{N_0\mu_n}[\Phi_{\mu_n}'(0)-\Phi_{\mu_n}''(0)]\int_{\rho_1}^{\rho_2}F_0(\mu_n\rho)F_\nu^2(\rho)\rho\,\mathrm{d}\rho\right\}\\ &= pq\left\{\frac{\rho_1}{\rho_2^2-\rho_1^2}\left[\int_{-\infty}^{0}f(s)\,\mathrm{d}s-f(0)\right]\right.\\ &\quad\left.+\frac{1}{\pi}\sum_{n=1}^{\infty}\frac{1}{N_0\mu_n}\left[\frac{4-\mu_n^2}{4-\mu_n}\int_{-\infty}^{0}f(s)\,e^{\mu_n s}\,\mathrm{d}s-f(0)\right]\int_{\rho_1}^{\rho_2}F_0(\mu_n\rho)F_\nu^2(\rho)\rho\,\mathrm{d}\rho\right\},\end{aligned} \tag{4.10}$$

where we have invoked (3.11) and (3.12); F_{11} represents the self-interaction of the cross-wave, and

$$\begin{aligned}\langle F_{11}\rangle &= \tfrac{1}{8}(p^2+q^2)^2\left\{\frac{2}{\rho_2^2-\rho_1^2}+\sum_{n=1}^{\infty}(4-\mu_n)\left[A_n\int_{\rho_1}^{\rho_2}F_0(\mu_n\rho)F_\nu^2(\rho)\rho\,\mathrm{d}\rho-A_n^2\right]\right.\\ &\quad+\frac{1}{2}\sum_{n=0}^{\infty}(4-\gamma_n)\left[B_n\int_{\rho_1}^{\rho_2}F_{2\nu}(\gamma_n\rho)F_\nu^2(\rho)\rho\,\mathrm{d}\rho-B_n^2\right]\\ &\quad+\frac{3}{16}\int_{\rho_1}^{\rho_2}\left[\left(\frac{\nu^4}{\rho^4}-\frac{2\nu^2}{\rho^2}-7\right)\tfrac{1}{2}F_\nu^4(\rho)+\frac{2\nu^2}{\rho^3}F_\nu^3(\rho)F_\nu'(\rho)\right.\\ &\quad\left.\left.+\left(3-\frac{11\nu^2}{\rho^2}\right)F_\nu^2(\rho)F_\nu'^2(\rho)+\frac{6}{\rho}F_\nu(\rho)F_\nu'^3(\rho)-\tfrac{3}{2}F_\nu'^4(\rho)\right]\rho\,\mathrm{d}\rho\right\}.\end{aligned} \tag{4.11}$$

We note that energy is transferred from the wavemaker to the radial cross-wave through the (spatial) mean motion of the free surface (cf. Garrett 1970). Additionally, energy is transferred via spatial coupling between the cross-wave and the directly forced wave. This spatial coupling is represented by an infinite sum over the axisymmetric free-modes (of zero spatial mean) in the annulus. We emphasize that, for every cross-wave in the annulus, energy is transferred from the wavemaker to the

cross-wave through this spatial coupling, in contrast to the two-dimensional cross-wave in a rectangular tank, for which this spatial coupling does not occur. This spatial coupling does occur for a three-dimensional cross-wave in a rectangular tank (see Appendix A).

Finally, we consider the wavemaker integral (4.2*b*). Invoking (1.1), (3.2), (3.5) and (2.4) for $\phi_{0_r}|_{r=r_1}$, we obtain

$$\langle W-W_0\rangle = \frac{2\epsilon^2 g\pi}{k_{\nu m}^4}\langle W_{10}\rangle + O(\epsilon^3), \tag{4.12}$$

where W_0 represents that part of W due to the directly forced wave, and

$$\langle W_{10}\rangle = pq\left\{\frac{\rho_1}{\rho_2^2-\rho_1^2}\int_{-\infty}^{0} f(s)\,\mathrm{d}s + \frac{2}{\pi}\sum_{n=1}^{\infty}\frac{A_n}{N_0\mu_n}\int_{-\infty}^{0} f(s)\,\mathrm{e}^{\mu_n s}\,\mathrm{d}s \right.$$
$$\left. + \frac{1}{\pi^2 N_\nu^2\rho_1}\left[\int_{-\infty}^{0}\mathrm{e}^{2s}\left[f'(s)+\left(1-\frac{\nu^2}{\rho_1^2}\right)f(s)\right]\mathrm{d}s\right]\right\}. \tag{4.13}$$

Combining the free-surface and wavemaker integrals, we obtain

$$\mathrm{L} \equiv \frac{\langle L-L_0\rangle}{\epsilon^2 g\pi/k_{\nu m}^4} = \tfrac{1}{2}(\dot{p}q-p\dot{q})+H, \tag{4.14}$$

where $L_0 = \frac{1}{2}(F_0+W_0)$ is the Lagrangian of the directly forced wave,

$$H = \tfrac{1}{2}\beta(p^2+q^2)+\Gamma_1 pq+\tfrac{1}{4}\Gamma_2(p^2+q^2)^2 \tag{4.15}$$

is a Hamiltonian,

$$\Gamma_1 \equiv \frac{2\rho_1}{\rho_2^2-\rho_1^2}\left[\int_{-\infty}^{0} f(s)\,\mathrm{d}s - \tfrac{1}{2}f(0)\right]$$
$$+\frac{2}{\pi}\sum_{n=1}^{\infty}\frac{1}{N_0\mu_n}\left[\frac{4-\mu_n^2}{4-\mu_n}\int_{-\infty}^{0} f(s)\,\mathrm{e}^{\mu_n s}\,\mathrm{d}s - \tfrac{1}{2}f(0)\right]\int_{\rho_1}^{\rho_2} F_0(\mu_n\rho)F_\nu^2(\rho)\rho\,\mathrm{d}\rho$$
$$+\frac{1}{\pi^2 N_\nu^2\rho_1}\left[\int_{-\infty}^{0}\mathrm{e}^{2s}\left[f'(s)+\left(1-\frac{\nu^2}{\rho_1^2}\right)f(s)\right]\mathrm{d}s\right] \tag{4.16a}$$

is a measure of the energy exchange between the wavemaker and the cross-wave, and

$$\Gamma_2 \equiv \frac{1}{2}\left\{\frac{2}{\rho_2^2-\rho_1^2}+\sum_{n=1}^{\infty}(4-\mu_n)\left[A_n\int_{\rho_1}^{\rho_2}F_0(\mu_n\rho)F_\nu^2(\rho)\rho\,\mathrm{d}\rho - A_n^2\right]\right.$$
$$+\frac{1}{2}\sum_{n=0}^{\infty}(4-\gamma_n)\left[B_n\int_{\rho_1}^{\rho_2}F_{2\nu}(\gamma_n\rho)F_\nu^2(\rho)\rho\,\mathrm{d}\rho - B_n^2\right]$$
$$+\frac{3}{16}\int_{\rho_1}^{\rho_2}\left[\left(\frac{\nu^4}{\rho^4}-\frac{2\nu^2}{\rho^2}-7\right)\tfrac{1}{2}F_\nu^4(\rho)+\frac{2\nu^2}{\rho^3}F_\nu^3(\rho)F_\nu'(\rho)\right.$$
$$\left.\left.+\left(3-\frac{11\nu^2}{\rho^2}\right)F_\nu^2(\rho)F_\nu'^2(\rho)+\frac{6}{\rho}F_\nu(\rho)F_\nu'^3(\rho)-\tfrac{3}{2}F_\nu'^4(\rho)\right]\rho\,\mathrm{d}\rho\right\} \tag{4.16b}$$

is a measure of the self-interaction of the cross-wave. We numerically evaluate the coefficient Γ_1, (4.16*a*), in Appendix C (see figure 6, table 2) for a particular wavemaker (C2).

5. Evolution equations

Invoking Hamilton's principle (that $\int \mathrm{L}\,d\tau$ be stationary with respect to independent variations of p and q), we obtain the evolution equations

$$\dot{p} = -\frac{\partial H}{\partial q} = -\Gamma_1 p - [\beta + \Gamma_2(p^2+q^2)]q, \tag{5.1a}$$

and

$$\dot{q} = \frac{\partial H}{\partial p} = \Gamma_1 q + [\beta + \Gamma_2(p^2+q^2)]p, \tag{5.1b}$$

which may be reduced to I (5.1) through the rescaling

$$(p, q) = \frac{1}{2\Gamma_2^{\frac{1}{2}}}(\hat{p}, \hat{q}), \quad \Gamma_1 = \beta_*, \tag{5.2a, b}$$

where we have assumed $\Gamma_2 > 0$. We incorporate linear damping by introducing $\alpha(p, q)$ on the left-hand sides of (5.1a, b), where

$$\alpha \equiv \delta/\epsilon, \tag{5.3}$$

and δ is the ratio of actual to critical damping (cf. I (5.7)), and obtain

$$\dot{p} = -\alpha p - \Gamma_1 p - [\beta + \Gamma_2(p^2+q^2)]q, \tag{5.4a}$$

and

$$\dot{q} = -\alpha q + \Gamma_1 q + [\beta + \Gamma_2(p^2+q^2)]p. \tag{5.4b}$$

For $\alpha < \Gamma_1$, the fixed points of (5.4), which correspond to harmonic motions ($\dot{p} = \dot{q} = 0$), are

$$p = q = 0, \tag{5.5}$$

$$p + \mathrm{i}q = \pm\Gamma_2^{-\frac{1}{2}} \exp[\mathrm{i}(\tfrac{3}{4}\pi - \psi)](\gamma - \beta)^{\frac{1}{2}} \quad (\beta < \gamma), \tag{5.6a}$$

$$p + \mathrm{i}q = \pm\Gamma_2^{-\frac{1}{2}} \exp[\mathrm{i}(\tfrac{1}{4}\pi + \psi)](-\gamma - \beta)^{\frac{1}{2}} \quad (\beta < -\gamma), \tag{5.6b}$$

where

$$\cos 2\psi \equiv \frac{\gamma}{\Gamma_1} = \left(1 - \frac{\alpha^2}{\Gamma_1^2}\right)^{\frac{1}{2}}, \tag{5.6c}$$

and

$$\gamma \equiv (\Gamma_1^2 - \alpha^2)^{\frac{1}{2}}. \tag{5.6d}$$

The linear stability analysis (cf. I §5) of these fixed points reveals that axisymmetric motions corresponding to (5.5) are stable/unstable if $\beta^2 \gtrless \gamma^2$ and that finite amplitude cross-waves corresponding to (5.6a/b) are stable/unstable. Hence, if $\beta > \gamma$, axisymmetric motions are stable; if $-\gamma < \beta < \gamma$, non-axisymmetric motions are stable; if $\beta < -\gamma$, either axisymmetric or non-axisymmetric motions are realizable depending upon the initial conditions. If $\alpha > \Gamma_1$, the only fixed point is $p = q = 0$, which is stable.

We remark that (5.1) are isomorphic to the equations governing Faraday resonance of surface waves in a basin subjected to vertical excitation (Miles 1984a, §§3–5).

6. Resonant forcing of the radial cross-wave and the directly forced wave

We now assume that the forcing frequency, 2ω, approximates both $2\omega_{\nu m}$ and ω_{0n} according to

$$\beta_1 \equiv \frac{\omega^2 - \omega_{\nu m}^2}{2\epsilon^{\frac{1}{2}}\omega^2} = \frac{1}{2\epsilon^{\frac{1}{2}}}\left[1 - \frac{k_{\nu m}}{\kappa}\right], \quad \beta_2 \equiv \frac{4\omega^2 - \omega_{0n}^2}{4\epsilon^{\frac{1}{2}}\omega^2} = \frac{1}{4\epsilon^{\frac{1}{2}}}\left[1 - \frac{\mu_n k_{\nu m}}{\kappa}\right], \tag{6.1a, b}$$

where μ_n is fixed by (3.9a), and choose an expansion of the form

$$\phi = \frac{\epsilon^{\frac{1}{2}} g}{k_{\nu m}\omega}(\phi_1 + \tfrac{1}{2}\phi_2), \quad \zeta = \frac{\epsilon^{\frac{1}{2}}}{k_{\nu m}}(\zeta_1 + \tfrac{1}{2}\zeta_2), \tag{6.2a, b}$$

where

$$\phi_1 = \mathrm{Re}\,[\{q_1(\tau) - \mathrm{i}p_1(\tau)\}\,\mathrm{e}^{-\mathrm{i}\omega t}]\,F_\nu(\rho)\cos\nu\theta\,\mathrm{e}^{\xi}, \tag{6.3a}$$

$$\zeta_1 = \mathrm{Re}\,[\{p_1(\tau) + \mathrm{i}q_1(\tau)\}\,\mathrm{e}^{-\mathrm{i}\omega t}]\,F_\nu(\rho)\cos\nu\theta, \tag{6.3b}$$

represent the cross-wave,

$$\phi_2 = \mathrm{Re}\,[\{q_2(\tau) - \mathrm{i}p_2(\tau)\}\,\mathrm{e}^{-2\mathrm{i}\omega t}]\,F_0(\mu_n\rho)\,\mathrm{e}^{\mu_n\xi}, \tag{6.4a}$$

$$\zeta_2 = \mathrm{Re}\,[2\{p_2(\tau) + \mathrm{i}q_2(\tau)\}\,\mathrm{e}^{-2\mathrm{i}\omega t}]\,F_0(\mu_n\rho), \tag{6.4b}$$

represent the directly forced wave and

$$\tau \equiv \epsilon^{\frac{1}{2}}\omega t. \tag{6.5}$$

Proceeding as in §4, and replacing μ_n by 4 except in β_j ($j = 1,2$), we obtain the average Lagrangian

$$\mathrm{L} \equiv \frac{\langle L\rangle}{\pi\epsilon^{\frac{3}{2}} g/k_{\nu m}^4} = \left[\frac{1}{2}\sum_{j-1}^{2}(\dot{p}_j q_j - p_j\dot{q}_j) + H\right], \tag{6.6a}$$

$$H = \frac{1}{2}\sum_{j-1}^{2}\beta_j(p_j^2 + q_j^2) - C[p_1 q_1 q_2 + \tfrac{1}{2}(p_1^2 - q_1^2)\,p_2] - Rq_2, \tag{6.6b}$$

where

$$C \equiv 3\int_{\rho_1}^{\rho_2} F_0(4\rho)\,F_\nu^2(\rho)\,\rho\,\mathrm{d}\rho, \quad R \equiv \frac{1}{2\pi N_0}\int_{-\infty}^{0} f(s)\,\mathrm{e}^{4s}\,\mathrm{d}s \tag{6.7a, b}$$

are a coupling coefficient and a measure of the energy transfer from the wavemaker to the directly forced wave.

Invoking Hamilton's principle and adding linear damping, we obtain the evolution equations,

$$\dot{p}_1 = -\alpha_1 p_1 - \beta_1 q_1 + C(p_1 q_2 - p_2 q_1), \tag{6.8a}$$

$$\dot{q}_1 = -\alpha_1 q_1 + \beta_1 p_1 - C(p_1 p_2 + q_1 q_2), \tag{6.8b}$$

$$\dot{p}_2 = -\alpha_2 p_2 - \beta_2 q_2 + C p_1 q_1 + R, \tag{6.8c}$$

$$\dot{q}_2 = -\alpha_2 q_2 + \beta_2 p_2 - \tfrac{1}{2}C(p_1^2 - q_1^2). \tag{6.8d}$$

Rescaling according to

$$\tau = R^{-1}\hat{\tau}, \quad \hat{\beta}_n = \frac{\beta_n}{R}, \quad \hat{\alpha}_n = \frac{\alpha_n}{R}, \quad (\hat{p}_j, \hat{q}_j) = \frac{C}{R}(p_j, q_j) \quad (j = 1,2), \tag{6.9a–d}$$

and dropping the hats, we obtain

$$\dot{p}_1 = -\alpha_1 p_1 - \beta_1 q_1 + p_1 q_2 - q_1 p_2, \tag{6.10a}$$

$$\dot{q}_1 = -\alpha_1 q_1 + \beta_1 p_1 - p_1 p_2 - q_1 q_2, \tag{6.10b}$$

$$\dot{p}_2 = -\alpha_2 p_2 - \beta_2 q_2 + p_1 q_1 + 1, \tag{6.10c}$$

$$\dot{q}_2 = -\alpha_2 q_2 + \beta_2 p_2 - \tfrac{1}{2}(p_1^2 - q_1^2), \tag{6.10d}$$

which may be transformed to the equations that govern two quadratically coupled oscillators (Miles 1984*b*, Appendix B) by a scale transformation followed by a canonical transformation similar to (7.7) below.

6.1. *Fixed points*

Setting the time derivatives in (6.10) equal to zero, we obtain the fixed points. We denote the solution

$$p_1 = q_1 = 0, \quad p_2 = \frac{\alpha_2}{\alpha_2^2+\beta_2^2}, \quad q_2 = \frac{\beta_2}{\alpha_2^2+\beta_2^2}, \tag{6.11a–c}$$

which corresponds to the directly forced wave, by P_0. We note that in the inviscid limit ($\alpha_1 = \alpha_2 = 0$), $q_2 \to \infty$ as $\beta_2 \to 0$.

The fixed points that correspond to a combination of the cross-wave and the directly forced wave are

$$p_1^2 = E_1 + P, \quad q_1^2 = E_1 - P, \tag{6.12a, b}$$

$$p_2 = \frac{1}{E_1}(\beta_1 P - \alpha_1 Q), \quad q_2 = \frac{1}{E_1}(\alpha_1 P + \beta_1 Q), \tag{6.12c, d}$$

where

$$P \equiv \tfrac{1}{2}(p_1^2 - q_1^2) = E_1(\alpha_1\beta_2 + \alpha_2\beta_1), \tag{6.13a}$$

$$Q \equiv p_1 q_1 = E_1(\beta_1\beta_2 - \alpha_1\alpha_2 - E_1), \tag{6.13b}$$

and

$$E_1 = \tfrac{1}{2}(p_1^2 + q_1^2) = \beta_1\beta_2 - \alpha_1\alpha_2 \pm [1 - (\alpha_1\beta_2 + \alpha_2\beta_1)^2]^{\frac{1}{2}}, \tag{6.14a}$$

$$E_2 = p_2^2 + q_2^2 = \alpha_1^2 + \beta_1^2 \tag{6.14b}$$

are the non-dimensional energies. We denote the fixed point that corresponds to the upper/lower choice of sign in (6.14*a*) by $P_\pm$.

The stability of the fixed points is determined by

$$D(s) = \begin{vmatrix} s_1 - q_2 & \beta_1 + p_2 & q_1 & -p_1 \\ -\beta_1 + p_2 & s_1 + q_2 & p_1 & q_1 \\ -q_1 & -p_1 & s_2 & \beta_2 \\ p_1 & -q_1 & -\beta_2 & s_2 \end{vmatrix} \tag{6.15a}$$

$$= s_1^2 s_2^2 + \beta_2^2 s_1^2 + (\beta_1^2 - E_2) s_2^2 + 4E_1 s_1 s_2 + 4E_1(E_1 - \beta_1\beta_2) - \beta_2^2 E_2 + \beta_1^2\beta_2^2 = 0, \tag{6.15b}$$

where $s_n \equiv s + \alpha_n$. Invoking (6.11), we obtain

$$D(s) = (s_1^2 + \beta_1^2 - E_2)(s_2^2 + \beta_2^2) = 0 \tag{6.16}$$

for P_0, which therefore is stable/unstable for

$$1 \lessgtr (\alpha_1^2 + \beta_1^2)(\alpha_2^2 + \beta_2^2). \tag{6.17}$$

Turning to the $P_\pm$, (6.12), we obtain

$$D(s) = s^4 + 2(\alpha_1 + \alpha_2) s^3 + [\alpha_2^2 + \beta_2^2 + 4(E_1 + \alpha_1\alpha_2)] s^2 + [2\alpha_1(\alpha_2^2 + \beta_2^2) + 4E_1(\alpha_1 + \alpha_2)] s + 4E_1(E_1 + \alpha_1\alpha_2 - \beta_1\beta_2) = 0. \tag{6.18}$$

Since $D(0) \gtrless 0$ for P_+/P_-, we conclude that P_- is always unstable.

The necessary and sufficient conditions for the stability of P_+ are

$$\alpha_2^2 + \beta_2^2 + 4(E_1 + \alpha_1\alpha_2) > 0, \quad 2\alpha_1(\alpha_2^2 + \beta_2^2) + 4E_1(\alpha_1 + \alpha_2) > 0, \tag{6.19a, b}$$

$$h = \frac{\alpha_1\alpha_2}{(\alpha_1+\alpha_2)^2}(\alpha_2^2+\beta_2^2)^2 + \frac{4\alpha_1^2\alpha_2(\alpha_2^2+\beta_2^2)}{\alpha_1+\alpha_2} + 2E_1[\alpha_2^2 + \beta_2^2 + 2(\beta_1\beta_2 + \alpha_1\alpha_2)] > 0. \tag{6.19c}$$

Equations (6.19*a*, *b*) are always satisfied. A necessary condition for (6.19*c*) to be violated is $\beta_1\beta_2 < 0$; then h may vanish and Hopf bifurcations may occur.

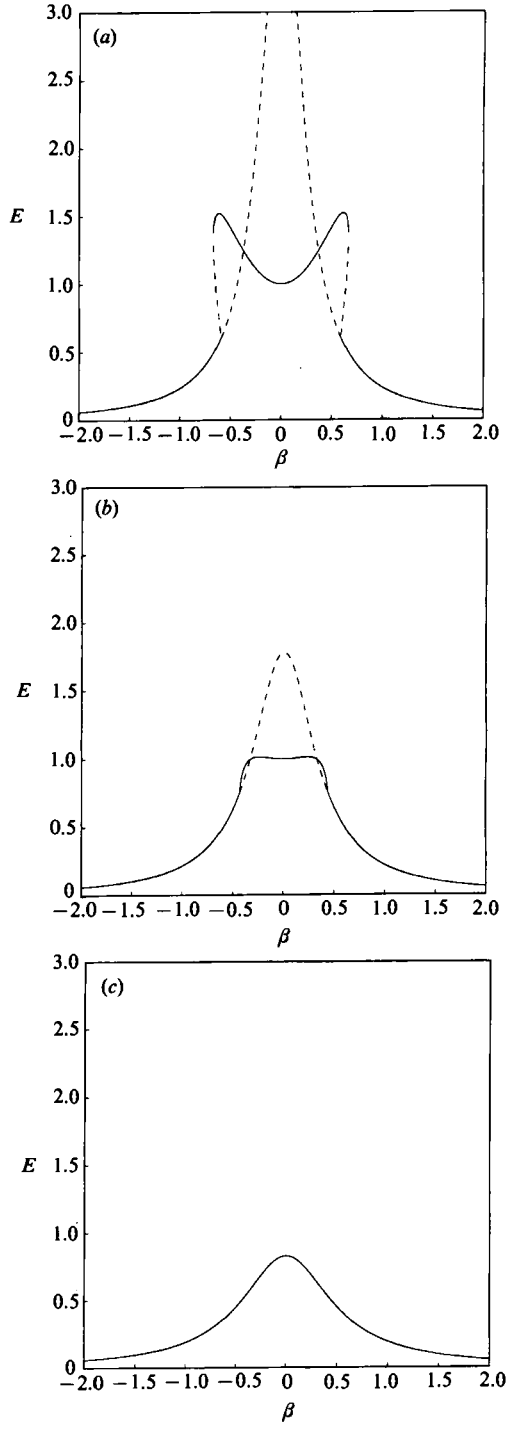

FIGURE 1. The dimensionless energy E (6.20) at the fixed points P_0 (6.11) and $P_\pm$ (6.14) versus the tuning parameter β, with $\Delta = 0$ ($\beta_1 = \frac{1}{2}\beta_2 \equiv \beta$), $\alpha_1 = \alpha_2 \equiv \alpha$ and (*a*) $\alpha = 0.5$, (*b*) $\alpha = 0.75$, and (*c*) $\alpha = 1.1$. The solid/dashed portions of the curves comprise stable/unstable equilibrium points.

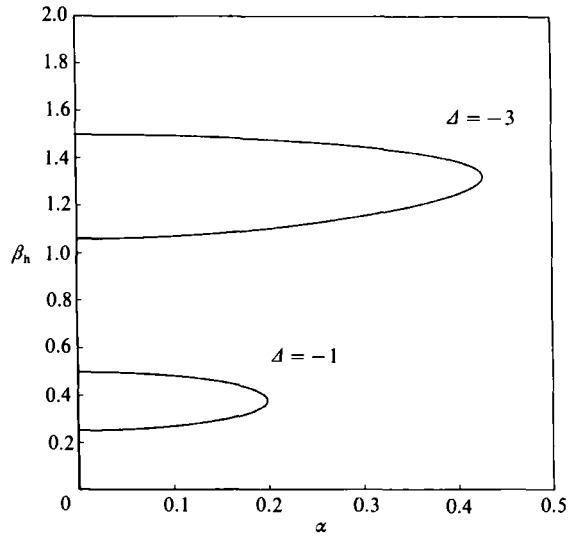

FIGURE 2. The Hopf bifurcation points for $\Delta = -1/-3$; the upper and lower Hopf bifurcations coalesce at $\beta_{hl} = \beta_{hu} = 0.38/1.32$ for $\alpha = 0.20/0.43$.

6.2. *Resonance curves*

We consider the resonance described by $\beta_1 = \frac{1}{2}(\beta_2 - \Delta) \equiv \beta$ on the simplifying assumption that $\alpha_1 = \alpha_2 \equiv \alpha$ in (6.10). The bifurcation diagrams are presented in the form of resonance curves: total dimensionless energy,

$$E = \tfrac{1}{2}(p_1^2 + q_1^2) + (p_2^2 + q_2^2), \tag{6.20}$$

at the fixed points P_0 (6.11) and $P_\pm$ (6.14) versus the tuning parameter β, with α and Δ as family parameters.

If $\Delta = 0$, the analysis follows that of Sethna (1965) and Miles (1984*b*). Then, (6.19) are satisfied, P_+ is always stable, and three distinct regions in α space exist in which the resonance curves exhibit qualitatively different characters.

If
$$\beta^2 = -\tfrac{5}{8}\alpha^2 + \tfrac{1}{8}(9\alpha^4 + 16)^{\frac{1}{2}} \equiv \beta_0^2, \tag{6.21}$$

no cross-wave is excited ($E_1 = p_1 = q_1 = 0$), symmetry-breaking bifurcations (at which axisymmetric solutions bifurcate to non-axisymmetric solutions) occur, and the condition for the stability of P_0 reduces to $|\beta| > |\beta_0|$.

If
$$\beta = \pm\frac{1}{3\alpha} \equiv \beta_{c\pm}, \tag{6.22}$$

turning-point bifurcations occur at which P_+ exchanges stability with P_-. Thus for $0 < \alpha < (\frac{2}{9})^{\frac{1}{4}}$, all of these bifurcation points exist (figure 1*a*). For $(\frac{2}{9})^{\frac{1}{4}} < \alpha < 1$, β_c and P_- are inadmissible (figure 1*b*). If $\alpha > 1$, β_0 is admissible and parametric excitation of the cross-wave is impossible; the resonance curves are those of a damped, resonantly forced, linear oscillator (figure 1*c*).

For $\Delta \neq 0$, the reflection symmetry of the resonance curves about $\beta = 0$ is broken and Hopf bifurcations may occur. We consider $\Delta < 0$ in the following; $\Delta \to -\Delta$ corresponds to $\beta \to -\beta$. We define $\beta_{hl/u}$ to be the smaller/larger value of β at which h (6.19*c*) vanishes. Figure 2 presents $\beta_{hl/u}$ versus α for $\Delta = -1/-3$; at $\alpha = 0.20/0.43$, the upper and lower Hopf-bifurcation points coalesce at $\beta_{hl} = \beta_{hu} = 0.38/1.32$.

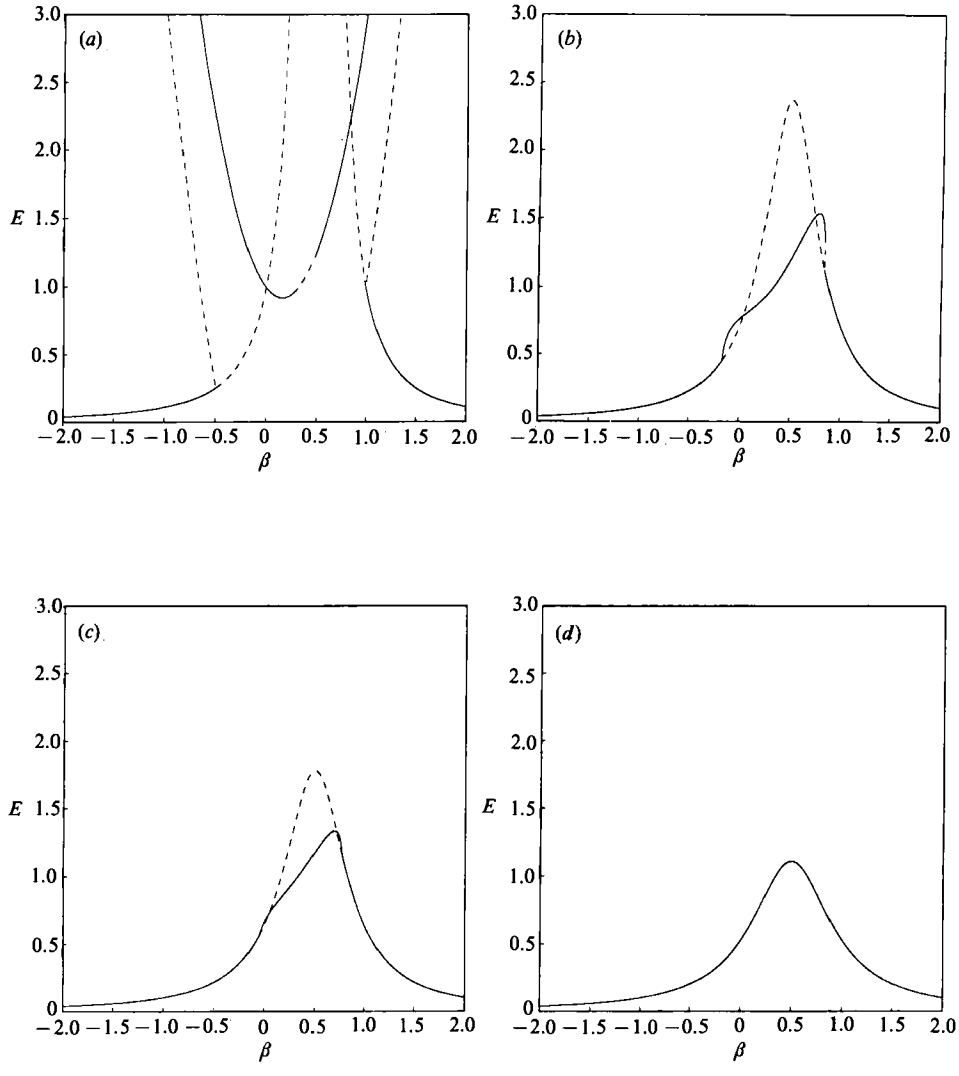

FIGURE 3. The dimensionless energy E (6.20) at the fixed points P_0 (6.11) and $P_\pm$ (6.14) versus the tuning parameter β, with $\Delta = -1$ ($\beta_1 = \frac{1}{2}[\beta_2 - \Delta] \equiv \beta$), $\alpha_1 = \alpha_2 \equiv \alpha$ and (*a*) $\alpha = 0.1$ (the turning-point bifurcations lie off the scale of the plot), (*b*) $\alpha = 0.65$, (*c*) $\alpha = 0.75$, and (*d*) $\alpha = 0.95$. The solid/dashed portions of the curves comprise stable/unstable equilibrium points.

The symmetry-breaking bifurcation point, β_0, now is determined by

$$4\beta_0^4 + 4\Delta\beta_0^3 + (5\alpha^2 + \Delta^2)\beta_0^2 + 4\alpha^2\Delta\beta_0 + \alpha^4 + \Delta^2\alpha^2 - 1 = 0. \tag{6.23}$$

There may be 0–4 real roots depending upon the values of Δ and α.

The turning-point bifurcations, (6.22), generalize to

$$\beta_{c\pm} = -\tfrac{1}{3}\Delta \pm \frac{1}{3\alpha}. \tag{6.24}$$

The resonance curves for $\Delta = -1$ are presented in figure 3 for four values of α. In contrast to $\Delta = 0$, we find intervals in β ($\beta_{h1} < \beta < \beta_{hu}$) for which no stable stationary solutions exist (cf. figure 3*a*).

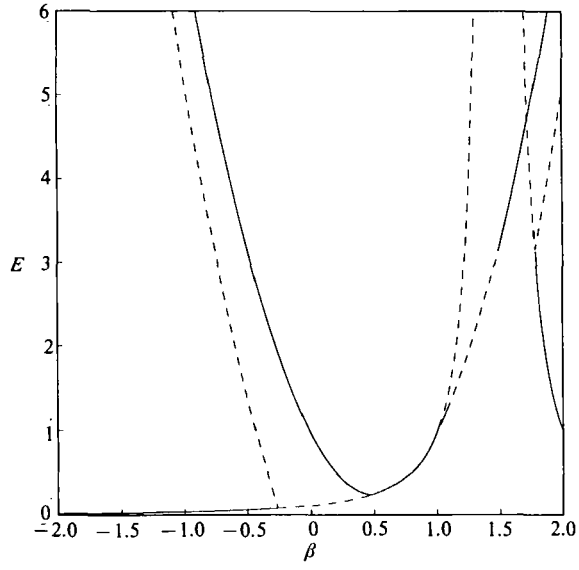

FIGURE 4. Resonance curves for $\Delta = -3$ and $\alpha = 0.1$ (see caption of figure 3).

The resonance curves for $\alpha = 0.1$ and $\Delta = -3$ are presented in figure 4, where four symmetry-breaking bifurcations occur.

6.3. *Numerical results*

Numerical integrations of (6.10) were performed using an Adams method. These runs typically were made for a total time $T = 2^{10}$, although near β_{hu}, some were made for $T = 2^{11}$. The points for which $0 \leqslant \tau < 2^9$ were removed from the time series of the total dimensionless energy E (6.20) in order to eliminate transient behaviour, after which the mean was removed. The power spectra of the resultant N-point time series of E were determined through a fast-Fourier-transform program according to

$$P(f_k) = (2\hat{\Delta}/N)\left|\sum_{n=0}^{N-1} E(\tau_n)\, w(\tau_n) \exp(-2\pi i f_k \tau_n)\right|^2, \tag{6.25}$$

where $f_k = k/T$ and $\tau_n = n\hat{\Delta}$ are the discrete dimensionless frequency and time, $\hat{\Delta}$ is the increment of τ, $T = N\hat{\Delta}$ is the length of the run, and

$$w(\tau) = (\tfrac{2}{3})^{\frac{1}{2}}[1 - \cos(2\pi\tau/T)] \tag{6.26}$$

is the normalized window function. Numerical noise was below $P = 10^{-10}$. The window function (6.26) introduced a small d.c.-component in the power spectra which was eliminated from figure 5 by omitting the first two ($k = 0, 1$) terms. We note that f_k in (6.25) is a scaled dimensionless frequency; the actual frequency of the slow modulations is $\epsilon^{\frac{1}{2}}\omega f_k$.

The parametric domain of principal interest for the numerical integrations is $\beta_{hl} < \beta < \beta_{hu}$, in which no stable fixed points exist. Runs were made for $\alpha = 0.1$, and $\Delta = -1$, $0.250 < \beta < 0.500$ ($\beta_{hl/u} = 0.272/0.484$), and $\Delta = -3$, $1.000 < \beta < 1.550$ ($\beta_{hl/u} = 1.072/1.495$). Initial conditions typically were $(p_1, q_1, p_2, q_2) = (0, 1, 0, 0)$; however, other values were explored.

For $\Delta = -1$ and $0.250 \leqslant \beta < 0.272$, the numerical runs spiralled into the stable fixed point P_+ for several choices of initial conditions. In contrast, for $\Delta = -3$ and

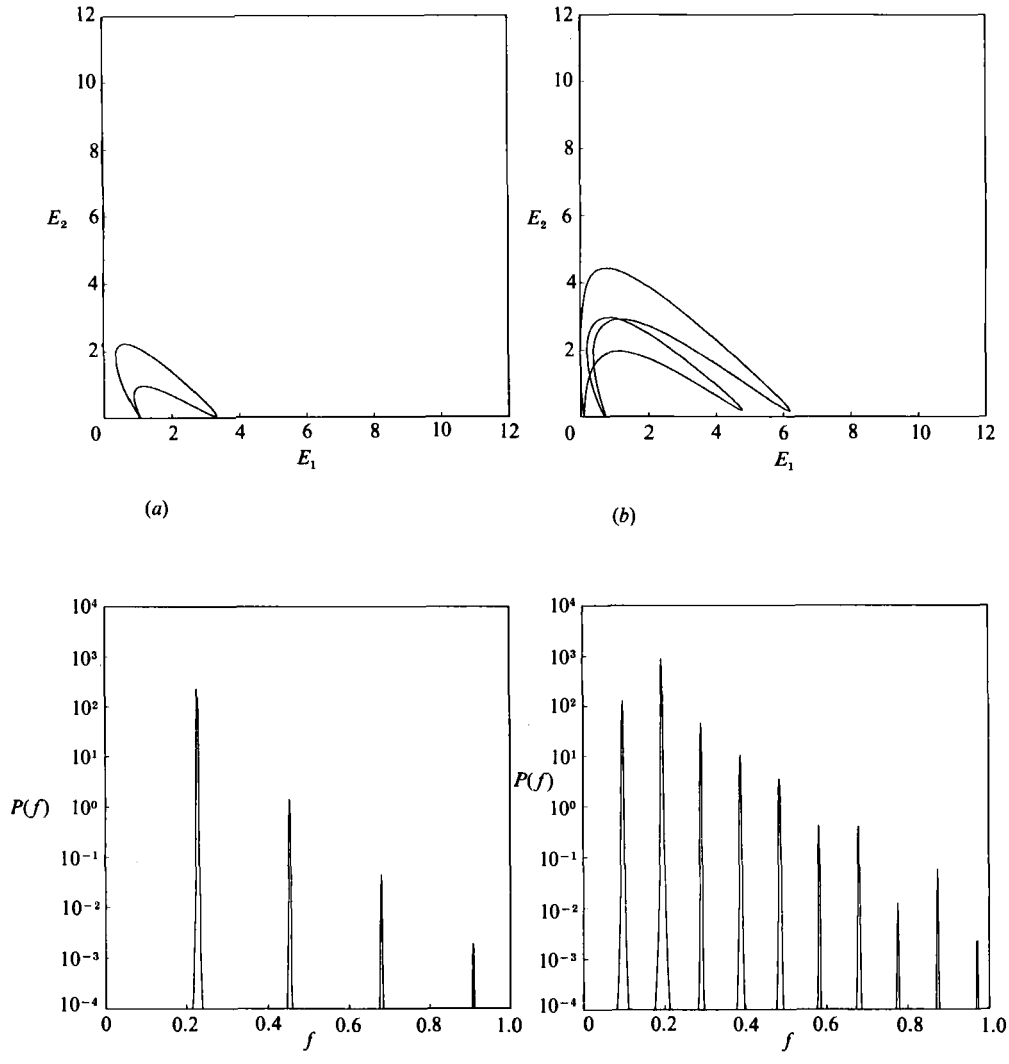

FIGURE 5(*a*, *b*). For caption see next page.

$1.055 \leqslant \beta < 1.072$, the numerical runs tended to either simple limit cycles or P_+, depending upon the initial conditions (for $\beta = 1.000$, the numerical runs terminated on P_0, see figure 4). This suggests, although we have not proved, that the lower Hopf bifurcation changes from super- to subcritical as Δ is decreased. For both values of Δ, increasing β above β_{hl} yielded simple limit cycles that subsequently underwent period-doubling cascades to chaos. Figure 5 presents this transition for $\Delta = -1$. Simple limit cycles were obtained for $\beta = 0.272, 0.280, 0.300, \ldots, 0.360, 0.380$ (figure 5*a*), period doubling for $\beta = 0.390, 0.395$ (figure 5*b*), period quadrupling for $\beta = 0.396$ (figure 5*c*), and chaotic trajectories for $\beta = 0.397, 0.400, 0.420, \ldots, 0.460, 0.480$ (figure 5*d*).

For both values of Δ and $\beta > \beta_{\mathrm{hu}}$, the numerical integrations spiralled into P_+. No simple limit cycles or period-doubling cascades were resolved as β was decreased through β_{hu}; chaotic trajectories were obtained for $\beta = 0.483/1.494$ for $\Delta = -1/-3$ respectively.

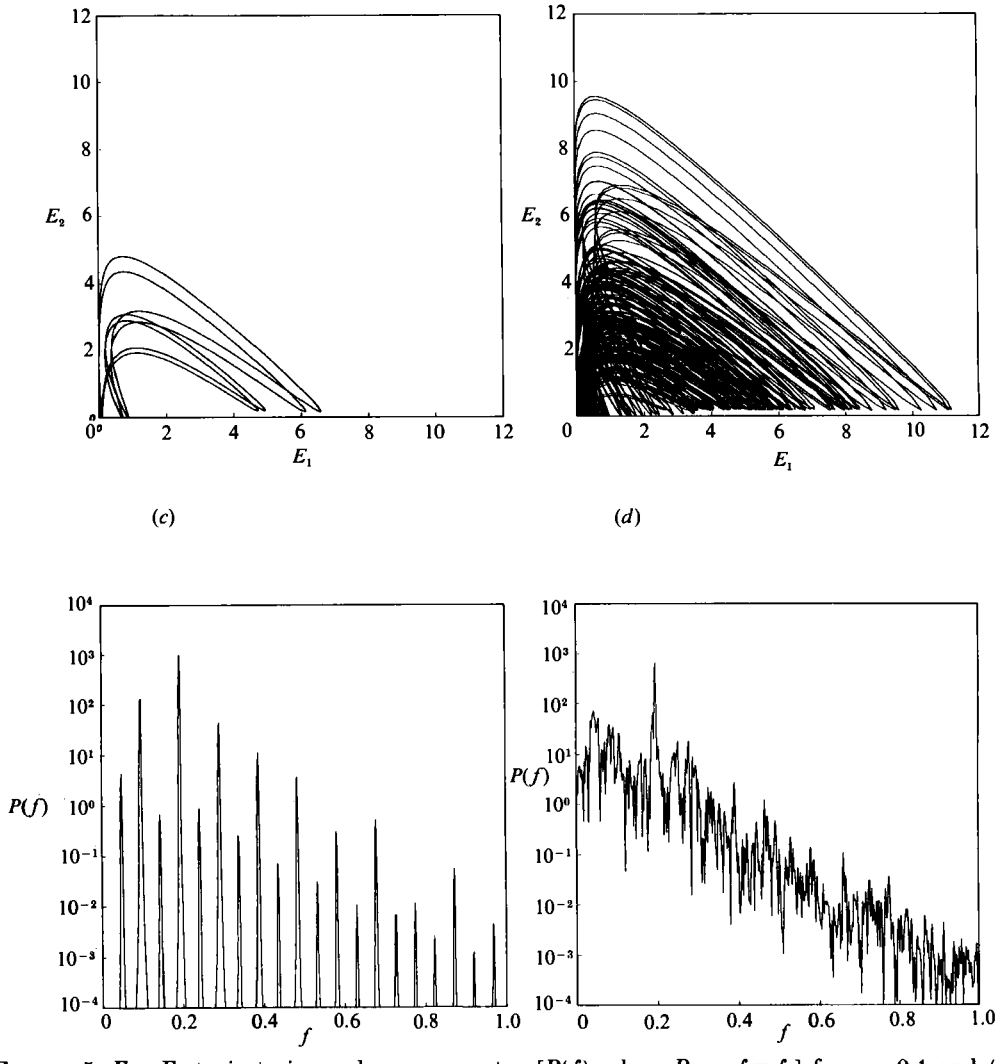

FIGURE 5. E_1-E_2 trajectories and power spectra $[P(f) = \log_{10} P$ *vs.* $f \equiv f_k]$ for $\alpha = 0.1$ and (*a*) $\beta = 0.300$, (*b*) $\beta = 0.395$, (*c*) $\beta = 0.396$, and (*d*) $\beta = 0.400$. The E_1-E_2 transients and the zero-frequency component of the power spectrum have been omitted. f is the scaled dimensionless frequency (see text).

7. 2:1 internal resonance; $2\omega \approx 2\omega_{\nu m} \approx \omega_{2\nu n}$

We now assume that the forcing frequency, 2ω, approximates both $2\omega_{\nu m}$ and $\omega_{2\nu n}$ according to

$$\beta_1 \equiv \frac{\omega^2-\omega_{\nu m}^2}{2\epsilon\omega^2} = \frac{1}{2\epsilon}\left[1-\frac{k_{\nu m}}{\kappa}\right], \quad \beta_2 \equiv \frac{4\omega^2-\omega_{2\nu n}^2}{4\epsilon\omega^2} = \frac{1}{4\epsilon}\left[4-\frac{\gamma_n k_{\nu m}}{\kappa}\right], \quad (7.1a, b)$$

where γ_n is fixed by (3.9*b*), and choose an expansion of the form

$$\phi = \frac{\epsilon g}{k_{\nu m}\omega}(2^{\frac{1}{2}}\phi_1+\phi_0+\phi_2), \quad \zeta = \frac{\epsilon}{k_{\nu m}}(2^{\frac{1}{2}}\zeta_1+\zeta_0+\zeta_2), \quad (7.2a, b)$$

where (ϕ_1, ζ_1) are given by (6.3), (ϕ_0, ζ_0) are given by (3.10), (ϕ_2, ζ_2) are given by

$$\phi_2 = \mathrm{Re}\,[\{q_2(\tau) - \mathrm{i}p_2(\tau)\}\,\mathrm{e}^{-2\mathrm{i}\omega t}]\,F_{2\nu}(\gamma_n \rho)\cos 2\nu\theta\,\mathrm{e}^{\gamma_n \xi}, \tag{7.3a}$$

$$\zeta_2 = \mathrm{Re}\,[2\{p_2(\tau) + \mathrm{i}q_2(\tau)\}\,\mathrm{e}^{-2\mathrm{i}\omega t}]\,F_{2\nu}(\gamma_n \rho)\cos 2\nu\theta, \tag{7.3b}$$

and τ is given by (3.3*e*) in (6.3) and (7.3). Proceeding as in §§4 and 6, we obtain the average Lagrangian

$$\mathrm{L} \equiv \frac{\langle L - L_0 \rangle}{4\pi g \epsilon^3 / k_{\nu m}^4} = \left[\frac{1}{2}\sum_{j=1}^{2}(\dot{p}_j q_j - p_j \dot{q}_j) + H\right], \tag{7.4a}$$

$$H = \frac{1}{2}\sum_{j=1}^{2}\beta_j(p_j^2 + q_j^2) + \Gamma_* p_1 q_1 - C_*[\tfrac{1}{2}(p_1^2 - q_1^2)\,p_2 + p_1 q_1 q_2], \tag{7.4b}$$

where

$$\Gamma_* \equiv \Gamma_1 - \frac{1}{\pi}\sum_{n=1}^{\infty}\frac{\mu_n}{N_0(4-\mu_n)}\left[\int_{-\infty}^{0} f(s)\,\mathrm{e}^{\mu_n s}\,\mathrm{d}s\right]\int_{\rho_1}^{\rho_2} F_0(\mu_n \rho)\,F_\nu^2(\rho)\,\rho\,\mathrm{d}\rho, \tag{7.5a}$$

$$C_* \equiv 3\int_{\rho_1}^{\rho_2} F_{2\nu}(4\rho)\,F_\nu^2(\rho)\,\rho\,\mathrm{d}\rho, \tag{7.5b}$$

and Γ_1 is given by (4.16*a*).

Invoking Hamilton's principle, we obtain

$$\dot{p}_1 = -\beta_1 q_1 - \Gamma_* p_1 + C_*(p_1 q_2 - q_1 p_2), \tag{7.6a}$$

$$\dot{q}_1 = \beta_1 p_1 + \Gamma_* q_1 - C_*(p_1 p_2 + q_1 q_2), \tag{7.6b}$$

$$\dot{p}_2 = -\beta_2 q_2 + C_* p_1 q_1, \tag{7.6c}$$

$$\dot{q}_2 = \beta_2 p_2 - \tfrac{1}{2}C_*(p_1^2 - q_1^2). \tag{7.6d}$$

The canonical transformation

$$\tau = \Gamma_*^{-1} T, \quad p_1 = \frac{\Gamma_*}{\sqrt{2C_*}}(P_1 - Q_1), \quad q_1 = \frac{\Gamma_*}{\sqrt{2C_*}}(P_1 + Q_1), \tag{7.7a–c}$$

$$p_2 = \frac{\Gamma_*}{C_*}Q_2, \quad q_2 = -\frac{\Gamma_*}{C_*}P_2, \tag{7.7d, e}$$

carries (7.4) over to

$$\hat{\mathrm{L}} = \frac{\Gamma_*^3}{C_*^2}\left[\frac{1}{2}\sum_{j=1}^{2}P_{j_T}Q_j - P_j Q_{j_T} + \hat{H}\right], \tag{7.8a}$$

$$\hat{H} = \frac{1}{2}\sum_{j=1}^{2}\frac{\beta_j}{\Gamma_*}(P_j^2 + Q_j^2) + \tfrac{1}{2}(P_1^2 - Q_1^2)(1 + P_2) + P_1 Q_1 Q_2, \tag{7.8b}$$

which is equivalent to 2:1 internal resonance for the Faraday problem (Miles 1984*a*, §6) with β_j replaced by β_j/Γ_* therein. Linear damping may be incorporated by introducing $(\alpha_1 p_1,\ \alpha_1 q_1,\ \alpha_2 p_2,\ \alpha_2 q_2)$ on the left-hand sides of (12.6*a–d*). These equations have been shown (Gu & Sethna 1987) to admit chaotic solutions for non-zero values of Δ, where $\Delta = \beta_2 - 2\beta_1$ (cf. §6)).

We thank Myrl Hendershott for many helpful discussions. This work was supported in part by the Physical Oceanography, Applied Mathematics and Fluid Dynamics/Hydraulics programs of the National Science Foundation, NSF Grant OCE-85-18763, by the Office of Naval Research, Contract N00014-84-K-0137, 4322318 (430), by the DARPA Univ. Res. Init. under Appl. and Comp. Math.

Program Contract N00014-86-K-0758 administered by the office of Naval Research, by a block grant of San Diego Super Computer Cray X-MP time, by a National Science Foundation graduate fellowship (J.M.B.) and by a grant under the Australian Research Council (J.M.B.).

Appendix A. Three-dimensional cross-waves in a rectangular tank

Following I and §§1–5, we examine the excitation of gravity waves in a short, rectangular tank of length l, breadth b and depth d by the wavemaker displacement

$$x = \chi = af(z)\sin 2\omega t \quad (0 < y < b, \quad -d < z < \zeta), \tag{A 1}$$

when ω approximates a natural frequency of a three-dimensional cross-wave,

$$\omega_{nm} = (gk_{nm})^{\frac{1}{2}} \equiv \left\{g\left[\left(\frac{n\pi}{b}\right)^2 + \left(\frac{m\pi}{l}\right)^2\right]\right\}^{\frac{1}{2}} \quad (n = 1, 2, \ldots, m = 1, 2, \ldots), \tag{A 2}$$

according to

$$\frac{\omega^2 - \omega_{nm}^2}{\omega^2} = 1 - \frac{k_{nm}}{\kappa} = O(\epsilon). \tag{A 3}$$

Garrett (1970), Miles (1988) and Tsai *et al.* (1990) have examined two-dimensional ($m = 0$) cross-waves.

We choose an expansion of the form (3.1) where the first-order cross-wave is given by

$$\phi_1 = \mathrm{Re}\,[\{q(\tau) - \mathrm{i}p(\tau)\}\,\mathrm{e}^{-\mathrm{i}\omega t}]\cos(K_1\hat{x})\cos(K_2\hat{y})\,\mathrm{e}^{\xi} \tag{A 4a}$$

$$\zeta_1 = \mathrm{Re}\,[\{p(\tau) + \mathrm{i}q(\tau)\}\,\mathrm{e}^{-\mathrm{i}\omega t}]\cos(K_1\hat{x})\cos(K_2\hat{y}), \tag{A 4b}$$

$$\hat{x} \equiv k_{nm}x, \quad \hat{y} \equiv k_{nm}y, \quad \xi \equiv k_{nm}z, \tag{A 5a–c}$$

$$K_1 \equiv \frac{m\pi}{k_{nm}l}, \quad K_2 \equiv \frac{n\pi}{k_{nm}b}, \quad K_1^2 + K_2^2 = 1, \tag{A 5d–f}$$

are dimensionless coordinates and horizontal wavenumbers, and τ is given by (3.3e). The second-order cross-wave (ϕ_{11}, ζ_{11}) is given by

$$\phi_{11} = \mathrm{Re}\,[\tfrac{1}{4}\mathrm{i}(p + \mathrm{i}q)^2\,\mathrm{e}^{-2\mathrm{i}\omega t}]\left\{\frac{1}{2} + \frac{K_1^2}{2 - K_2}\cos(2K_2\hat{y})\,\mathrm{e}^{2K_2\xi} + \frac{K_2^2}{2 - K_1}\cos(2K_1\hat{x})\,\mathrm{e}^{2K_1\xi}\right\}, \tag{A 6a}$$

$$\begin{aligned}\zeta_{11} = \mathrm{Re}\,[\tfrac{1}{8}(p + \mathrm{i}q)^2\,\mathrm{e}^{-2\mathrm{i}\omega t}]&\left\{\left[\frac{K_2[K_2^2 - 2(1 - K_2)]}{2 - K_2}\right]\cos(2K_2\hat{y})\right.\\ &\left. + \left[\frac{K_1[K_1^2 - 2(1 - K_1)]}{2 - K_1}\right]\cos(2K_1\hat{x}) + \cos(2K_1\hat{x})\cos(2K_2\hat{y})\right\}\\ &+ \tfrac{1}{8}(p^2 + q^2)\{K_2^2\cos(2K_2\hat{y}) + K_1^2\cos(2K_1\hat{x}) + \cos(2K_1\hat{x})\cos(2K_2\hat{y})\}.\end{aligned} \tag{A 6b}$$

We obtain the simpler, two-dimensional result I (3.5), wherein ϕ_{11} is a pure function of time and represents a spatially uniform pressure oscillating at the wavemaker frequency, by setting $K_1 = 0$ in (A 6) and allowing for the different normalizations of the first-order cross-wave (the present (p, q) is replaced by $\sqrt{2}(p, q)$ in I). We remark that, in contrast to the radial cross-wave problem (cf. (3.5)), internal resonance between a rectangular cross-wave and its second harmonic cannot occur, by virtue of which $(\phi_{11}, \zeta_{11}) = O(1)$ for all K_1, K_2.

The directly forced wave is given by

$$\phi_0 = \cos 2\omega t\left[\frac{\Phi_0(\xi)}{\kappa l}+\frac{2}{\kappa l}\sum_{m'=1}^{\infty}\Phi_{\nu_{m'}}(\xi)\cos(\nu_{m'}\hat{x})\right] \tag{A 7a}$$

and

$$\zeta_0 = 2\sin 2\omega t\left[\frac{\Phi_0(0)}{\kappa l}+\frac{2}{\kappa l}\sum_{m'=1}^{\infty}\Phi_{\nu_{m'}}(0)\cos(\nu_{m'}\hat{x})\right], \tag{A 7b}$$

where $\nu_{m'} = m'\pi/\kappa l$, and the $\Phi_{\nu_{m'}}(\xi)$, $m' = 0, 1, \ldots, \infty$, are given in Appendix B. We anticipate that the only terms in the series (A 7) needed here are given by (3.11) and

$$\Phi_{\nu_{2m}}(0) = \frac{1}{2-K_1}\int_{-\infty}^{0} f(s)\,\mathrm{e}^{2K_1 s}\,\mathrm{d}s, \quad \Phi'_{\nu_{2m}}(0) = 4\Phi_{\nu_{2m}}(0), \tag{A 8a, b}$$

$$\Phi''_{\nu_{2m}}(0) = 4K_1^2\Phi_{\nu_{2m}}(0)+2f(0). \tag{A 8c}$$

Following §4, we calculate the average Lagrangian, which may be reduced to integrals over the rest position of the free surface and the wavemaker (cf. (4.6)). In the calculation of the free-surface integral, F_1 is given by (4.8) with $\omega_{\nu m}$ and $k_{\nu m}$ defined by (A 2), (4.10) is replaced by

$$\begin{aligned}\langle F_{10}\rangle &= \frac{pq}{4\kappa l}[\Phi'_0(0)-\Phi''_0(0)+(\Phi'_{\nu_{2m}}(0)-\Phi''_{\nu_{2m}}(0))]\\ &= \frac{pq}{2\kappa l}\left\{\int_{-\infty}^{0} f(s)\,\mathrm{d}s-f(0)+\frac{2K_2^2}{2-K_1}\int_{-\infty}^{0} f(s)\,\mathrm{e}^{2K_1 s}\,\mathrm{d}s-f(0)\right\},\end{aligned} \tag{A 9}$$

where we have invoked (3.11) and (A 8), and (4.11) is replaced by

$$\langle F_{11}\rangle = \left[\frac{(p^2+q^2)^2}{128}\right]\left\{7-8\left[\frac{K_1^4}{2-K_2}+\frac{K_2^4}{2-K_1}\right]-6K_1^2K_2^2\right\}. \tag{A 10}$$

Comparing (4.10) with (A 9), we note that, for both radial cross-waves and three-dimensional cross-waves in a rectangular tank, energy is transferred from the wavemaker to the cross-wave through the (spatial) mean motion of the free surface and through spatial coupling between the cross-wave and the directly forced wave. For radial cross-waves, this spatial coupling is represented by an infinite sum over the axisymmetric free modes in an annulus, whereas for three-dimensional cross-waves in a rectangular tank, it occurs only between the cross-wave and the $2m$-Fourier-cosine component of the directly forced wave. This spatial coupling does not occur for two-dimensional ($m = 0$) cross-waves in a rectangular tank. We emphasize, however, that owing to the spatial integrations, the two-dimensional limit ($m \to 0$) of $\langle L\rangle$ is not uniformly valid.

For the wavemaker integral (4.13) is replaced by

$$\langle W_{10}\rangle = \frac{pq}{2\kappa l}\left\{\int_{-\infty}^{0} f(s)\left[1+\frac{2K_2^2}{(2-K_1)}\mathrm{e}^{2K_1 s}\right]\mathrm{d}s+\int_{-\infty}^{0}\mathrm{e}^{2s}[K_1^2 f(s)+f'(s)]\,\mathrm{d}s\right\}. \tag{A 11}$$

Combining the free surface and wavemaker integrals, we obtain

$$\mathrm{L} \equiv \frac{\langle L-L_0\rangle}{\frac{1}{4}a^2gbl} = \tfrac{1}{2}(\dot{p}q-p\dot{q})+H, \tag{A 12}$$

where $L_0 = \frac{1}{2}(F_0 + W_0)$ is the Lagrangian of the directly forced wave, H is given by (4.15) with (4.16) replaced by

$$\Gamma_1 \equiv \frac{1}{\kappa l}\left\{\int_{-\infty}^{0} f(s)\,\mathrm{d}s - \tfrac{1}{2}f(0) + \frac{2K_2^2}{2-K_1}\int_{-\infty}^{0} f(s)\,\mathrm{e}^{2K_1 s}\,\mathrm{d}s - \tfrac{1}{2}f(0) + \frac{1}{2}\int_{-\infty}^{0} \mathrm{e}^{2s}[K_1^2 f(s) + f'(s)]\,\mathrm{d}s\right\}, \quad \text{(A 13}a\text{)}$$

and

$$\Gamma_2 \equiv \frac{1}{32\kappa l}\left\{7 - 8\left[\frac{K_1^4}{2-K_2} + \frac{K_2^4}{2-K_1}\right] - 6K_1^2K_2^2\right\}. \quad \text{(A 13}b\text{)}$$

The evolution equations that govern (p, q) for three-dimensional cross-waves in a rectangular tank are given by (5.1) with the changes in the coefficients indicated above. The stability analysis of §5 also carries over.

Appendix B. The directly forced wave

The directly forced wave satisfies

$$\nabla^2\phi_0 = 0, \quad \text{(B 1)}$$

$$\phi_{0_\xi} = \omega^{-1}\zeta_{0_t} \quad (\xi = 0), \quad \omega^{-1}\phi_{0_t} = -\zeta_0 \quad (\xi = 0), \quad \phi_{0_\xi} \to 0 \quad (\xi \downarrow -\infty), \quad \text{(B 2}a\text{–}c\text{)}$$

$$\phi_{0_\rho} = 2f(\xi)\cos 2\omega t \quad (\rho = \rho_1), \quad \phi_{0_\rho} = 0 \quad (\rho = \rho_2). \quad \text{(B 3}a, b\text{)}$$

We define the finite Hankel transform,

$$G_{\mu_n}(\xi) = \int_{\rho_1}^{\rho_2} g(\rho, \xi)\,F_0(\mu_n\rho)\,\rho\,\mathrm{d}\rho, \quad \text{(B 4}a\text{)}$$

$$g(\rho, \xi) = \frac{\sqrt{2}}{(\rho_2^2 - \rho_1^2)^{\frac{1}{2}}}G_0(\xi) + \sum_{n=1}^{\infty} G_{\mu_n}(\xi)\,F_0(\mu_n\rho), \quad \text{(B 4}b\text{)}$$

where

$$F_0(\mu_0\rho) = \frac{\sqrt{2}}{(\rho_2^2 - \rho_1^2)^{\frac{1}{2}}} \quad (\mu_0 \equiv 0),$$

and the $F_0(\mu_n\rho)$, $(n = 1, 2, \ldots)$ are given by (3.7a). Applying (B 4a) to (B 1)–(B 3), we obtain

$$P_{\mu_n\xi\xi} - \mu_n^2 P_{\mu_n} = 2\rho_1 F_0(\mu_n\rho_1)f(\xi), \quad \text{(B 5)}$$

$$-4P_{\mu_n} + P_{\mu_n\xi} = 0 \quad (\xi = 0), \quad P_{\mu_n\xi} \to 0 \quad (\xi \downarrow -\infty), \quad \text{(B 6}a, b\text{)}$$

where we have eliminated ζ_0 from (B 2a, b) in favour of ϕ_0 and separated out the $\mathrm{e}^{-2\mathrm{i}\omega t}$ time dependence.

Solving (B 5) and (B 6) and invoking (B 4b), we obtain

$$\phi_0 = \cos 2\omega t\left[\frac{\sqrt{2}}{(\rho_2^2 - \rho_1^2)^{\frac{1}{2}}}P_0(\xi) + \sum_{n=1}^{\infty} P_{\mu_n}(\xi)\,F_0(\mu_n\rho)\right], \quad \text{(B 7)}$$

where

$$P_0(\xi) = \frac{\sqrt{2}\rho_1}{(\rho_2^2 - \rho_1^2)^{\frac{1}{2}}}\left[\int_{-\infty}^{0} f(s)\,(\tfrac{1}{2} + 2\xi)\,\mathrm{d}s + 2\int_{\xi}^{0} f(s)\,(s - \xi)\,\mathrm{d}s\right] \equiv \frac{\sqrt{2}\rho_1}{(\rho_2^2 - \rho_1^2)^{\frac{1}{2}}}\Phi_0(\xi), \quad \text{(B 8}a\text{)}$$

and

$$P_{\mu_n}(\xi) = \frac{2}{\pi\mu_n^2 N_0}\left\{\left[\frac{4+\mu_n}{4-\mu_n}\right]\int_{-\infty}^{0} f(s)\,\mathrm{e}^{\mu_n(\xi+s)}\,\mathrm{d}s - \int_{\xi}^{0} f(s)\,\mathrm{e}^{\mu_n(\xi-s)}\,\mathrm{d}s \right.$$
$$\left. - \int_{-\infty}^{\xi} f(s)\,\mathrm{e}^{-\mu_n(\xi-s)}\,\mathrm{d}s\right\} \equiv \frac{2}{\pi\mu_n N_0}\Phi_{\mu_n}(\xi). \quad \text{(B 8}b\text{)}$$

For cross-waves in a rectangular tank, the directly forced wave satisfies (B 1) and (B 2) with (B 3) replaced by

$$\phi_{0_{\hat{x}}} = 2f(\xi)\cos 2\omega t \quad (\hat{x}=0), \quad \phi_{0_{\hat{x}}} = 0 \quad (\hat{x}=\kappa l). \quad \text{(B 9}a, b\text{)}$$

We define the finite-cosine transform,

$$G_{\upsilon_{m'}}(\xi) = \int_0^{\kappa l} g(\hat{x},\xi)\cos(\upsilon_{m'}\hat{x})\,d\hat{x}, \quad \text{(B 10}a\text{)}$$

$$g(\hat{x},\xi) = \frac{1}{\kappa l}G_0(\xi) + \frac{2}{\kappa l}\sum_{m'=1}^{\infty} G_{\upsilon_{m'}}(\xi)\cos(\upsilon_{m'}\hat{x}), \quad \text{(B 10}b\text{)}$$

where
$$\upsilon_{m'} \equiv \frac{m'\pi}{\kappa l}. \quad \text{(B 10}c\text{)}$$

The equations that correspond to (B 5) and (B 6) are

$$\Phi_{\upsilon_{m'}\xi\xi}(\xi) - \upsilon_{m'}^2\Phi_{\upsilon_{m'}}(\xi) = 2f(\xi), \quad \text{(B 11)}$$

$$-4\Phi_{\upsilon_{m'}}(\xi) + \Phi_{\upsilon_{m'}\xi}(\xi) = 0 \quad (\xi=0), \quad \Phi_{\upsilon_{m'}\xi}(\xi)\to 0 \quad (\xi\downarrow -\infty). \quad \text{(B 12}a, b\text{)}$$

Solving (B 11) and (B 12) and invoking (B 10b), we obtain

$$\phi_0 = \cos 2\omega t\left[\frac{\Phi_0(\xi)}{\kappa l} + \frac{2}{\kappa l}\sum_{m'=1}^{\infty}\Phi_{\upsilon_{m'}}(\xi)\cos(\upsilon_{m'}\hat{x})\right], \quad \text{(B 13)}$$

where $\Phi_0(\xi)$ is given by (B 8a) and $\Phi_{\upsilon_{m'}}(\xi)$ is given by (B 8b).

Appendix C. Experiments

By Janet M. Becker and Diane M. Henderson†

We conducted preliminary experiments on standing radial cross-waves by subjecting a floating ping-pong ball ($r_1 = 1.89$ cm) to vertical oscillation in a Pyrex beaker ($r_2 = 4.25$ cm) that contained a distilled water/Kodak Photo Flo solution. The static surface tension at the fluid–air interface was $T = 42.3$ dyn/cm. Because of the small scale of these experiments, surface tension must be incorporated in the deep-water dispersion relationship according to

$$\omega^2 = g\kappa + T\kappa^3, \quad \omega = 2\pi f, \quad \text{(C 1}a\text{)}$$

† Institute of Geophysics and Planetary Physics, University of California, La Jolla, CA 92093, USA.

Expt no.	f_0 (Hz)	f_1 (Hz)	a_0 (mm)	κ (cm^{-1})	ν
1	12.019	6.010	0.94	1.35	1
2	12.520	6.260	0.94	1.45	1
3	13.021	6.510	0.88	1.55	2
4*a*	13.516	6.758	0.88	1.65	1
4*b*	13.516	6.758	0.95	1.65	2
5	14.001	7.005	0.88	1.74	3
6	14.521	7.261	0.88	1.85	3
7	15.024	7.512	0.81	1.95	4
8	15.501	7.751	0.82	2.05	4–5[a]
9	16.009	8.005	0.81	2.15	5
10*a*	16.552	8.276	0.81	2.26	[b]
10*b*	16.552	8.276	0.90	2.26	[b]
11	17.058	8.529	0.83	2.36	5
12	17.517	8.758	0.83	2.45	5
13*a*	18.001	9.006	0.82	2.55	[b]
13*b*	18.001	9.006	0.84	2.55	[b]
14*a*	18.513	9.257	0.83	2.65	[c]
14*b*	18.513	9.257	0.84	2.65	[c]
15	19.055	9.527	0.83	2.75	6
16	19.531	9.766	0.84	2.85	[b]
17	20.032	10.016	0.82	2.94	7–8[a]
18	25.040	12.520	0.88	3.85	7–8[a]

[a] Uncertain azimuthal mode number (no consensus reached between observers).
[b] Irregular wavefield, no single cross-wave mode observed.
[c] Steady superposition of a $\nu = 3$ mode and a $\nu = 6$ mode.

TABLE 1. Experiments on standing cross-waves

and
$$\omega_{\nu m}^2 = gk_{\nu m} + Tk_{\nu m}^3. \qquad (C\,1b)$$

We note that $\kappa d = O(10)$ so that the deep-water assumption is justified. The electronics that drove the ping-pong ball and measured the wavemaker and wavefield amplitudes and frequencies are described in Henderson & Miles (1989).

The experiments were conducted as follows. We fixed the driving frequency and increased the wavemaker stroke until a finite-amplitude radial cross-wave was observed.† We measured an *in situ* time-series of the surface displacement and determined its frequency content with an energy spectrum. We then computed the radial wavenumber κ of the cross-wave from (C 1*a*). We determined the azimuthal wavenumber ν of the cross-wave by independently counting the number of wavelengths around the ball. Table 1 presents the measured wavemaker frequency f_0, cross-wave frequency f_1, wavemaker amplitude a_0, and the radial and azimuthal wavenumbers of the cross-wave. We observed a single cross-wave mode for driving frequencies in 12 Hz $< f_0 <$ 16 Hz; it was typically steady, but sometimes rotated slowly around the ball at the higher frequencies. The surface displacement was irregular for some values of $f_0 >$ 16 Hz. This spatial disorder may be due to 2:1 resonances, as described in §§6 and 7, or to mode competition, (cf. Ciliberto & Gollub 1985), as the natural frequencies for different cross-wave modes become closely spaced as f is increased (see figure 7). We observed a steady superposition of a $\nu = 3$ mode and $\nu = 6$ mode for $f_0 = 18.513$ Hz. Further experiments are needed to determine whether this is a 1:1 internal resonance between a (3, 2) and a (6, 1) mode

† We did not attempt to measure the wavemaker amplitude at which the cross-wave is neutrally stable.

ν, m	$k_{\nu m}$	Γ_1	ν, m	$k_{\nu m}$	Γ_1
1,0	0.33	[a]	6,0	1.76	0.22
1,1	1.41	0.31	6,1	2.68	0.46
1,2	2.70	0.37	6,2	3.50	0.53
1,3	4.02	0.40	6,3	4.56	0.47
2,0	0.65	0.24	7,0	2.02	0.19
2,1	1.56	0.37	7,1	2.99	0.33
2,2	2.78	0.39	7,2	3.77	0.56
2,3	4.06	0.40	7,3	4.75	0.50
3,0	0.95	0.21	8,0	2.27	0.20
3,1	1.79	0.45	8,1	3.29	0.37
3,2	2.89	0.41	8,2	4.06	0.57
3,3	4.15	0.41	8,3	4.96	0.52
4,0	1.23	0.24	9,0	2.52	0.21
4,1	2.07	0.49	9,1	3.58	0.33
4,2	3.05	0.46	9,2	4.32	0.56
4,3	4.25	0.43	9,3	5.20	0.56
5,0	1.50	0.22			
5,1	2.37	0.49			
5,2	3.26	0.49			
5,3	4.39	0.45			

[a] $\mu_1 = 4.10$ see §6.

TABLE 2. Numerical values of Γ_1 for $r_1 = 1.89$ and $r_2 = 4.25$

or a 2:1 internal resonance between a (3,2) and a (6,4) mode for which the theory of §7 applies. We note that in the resonance conditions (7.1), $\omega/\omega_{\nu m}$ are defined by (C 1*a*, *b*).

The theory of §§1–7 is for a cylindrical, rather than a spherical, wavemaker; accordingly, we attempt only a qualitative comparison between theory and experiment. We compute the stability of the axisymmetric directly forced wave and the cross-wave for the experiments in which we observed a single cross-wave mode. To this end, we numerically evaluate the interaction coefficients Γ_1 and Γ_2. As we are not attempting to compare the predicted wave-field amplitudes with the experimental data, only the sign of Γ_2 is needed. We compute Γ_2 from (4.16*b*) for $m = 1$, $\nu = 1$–6. The two infinite sums in (4.16*b*) typically converge to three places after the first few terms although fifteen terms were computed, and Γ_2 is always positive for these cases; hence, the stability analysis of §5 carries over directly.

We compute Γ_1 from (4.16*a*) by choosing a simple analytic function for the wavemaker shape:

$$f(\xi) = \frac{a_w + b_w}{b_w} e^{a_w/k_{\nu m}\xi} - \frac{a_w}{b_w} e^{(a_w+b_w)/k_{\nu m}\xi}; \tag{C 2}$$

we note that $f'(0) = 0$ and $f(\xi) \downarrow 0$, $\xi \downarrow -\infty$. Table 2 presents Γ_1 for the $f(\xi)$ given by (C 2) with $a_w = b_w = 1$ and $0 \leqslant m \leqslant 3$, $1 \leqslant \nu \leqslant 9$. We note that for the (1,0) mode, $\mu_1 = 4.10$; hence, the single-mode theory is invalid (cf. §6). The first term in (4.16*a*), which represents the coupling between the cross-wave and the spatially averaged motion of the directly forced wave, is the dominant contribution to Γ_1. For a fixed ν, this term increases with increasing m. The second term in (4.16*a*), the infinite sum, which represents coupling between the cross-wave and the axisymmetric free modes

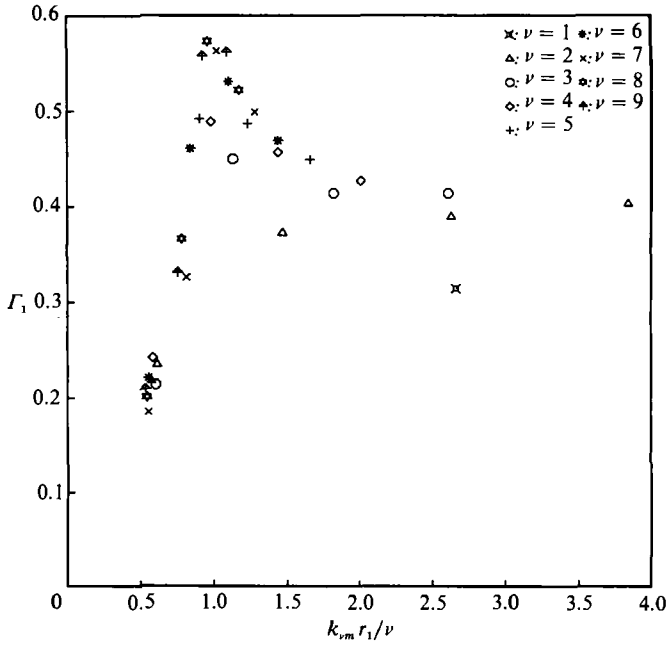

FIGURE 6. Γ_1 *vs.* $k_{\nu m} r_1/\nu$ where Γ_1 is given by (4.16*a*) and $f(\xi)$ is given by (C 2) with $a_w = b_w = 1$.

(of zero spatial mean) in an annulus, typically converged to two places after a few terms, although between ten and twenty terms were computed. For $\nu = 1$ and $3 \leqslant \nu \leqslant 8$, the radial mode number dependence of this sum is such that the maximum of Γ_1 and this sum coincide. The last term (4.16*a*), which arises from nonlinearity in the wavemaker boundary condition (2.4), is typically small and weakly dependent upon radial mode number as it crosses zero from below as m is increased. Figure 6 presents Γ_1 versus $k_{\nu m} r_1/\nu$ for $\nu = 1$–9. We note that for $3 \leqslant \nu \leqslant 9$, Γ_1 exhibits a maximum near $k_{\nu m} \approx \nu/r_1$, the turning point of Bessel's equation (i.e. when the wavemaker is near the turning point of the cross-wave radial profile (3.4*a*)).

The boundary above which axisymmetric motions are unstable with respect to cross-wave perturbations is given by (cf. §5)

$$a = \frac{1}{k_{\nu m} \Gamma_1}\left[\delta^2 + \frac{(\omega^2 - \omega_{\nu m}^2)^2}{(2\omega^2)^2}\right]^{\frac{1}{2}} \equiv a_m. \tag{C 3}$$

In addition, a finite-amplitude cross-wave is stable if $\omega < \omega_{\nu m}$ or if $\omega > \omega_{\nu m}$ and $a > a_m$. We measured the dissipation parameter $\delta = 0.035$ for experiment 6 only, and that value is used in the computation (C 3) for all the experiments. Figure 7 presents a_m versus $\omega/2\pi$ as given by (C 3). Superimposed on these curves are the (f_1, a_0) coordinates of the experiments. The theory is in agreement with the experiments in predicting that the observed cross-wave is stable except for experiment 4*a*, for which the cross-wave is unstable. For the majority of the experiments for which the cross-wave is stable (experiments 2, 3, 4*b*–7, the (4, 1) mode of 8†, 9, 11, 12, 15, the (7, 1) mode of 17† and 18), the axisymmetric, directly forced wave is unstable. For

† As noted in table 1, the azimuthal wavenumber in this experiment is uncertain.

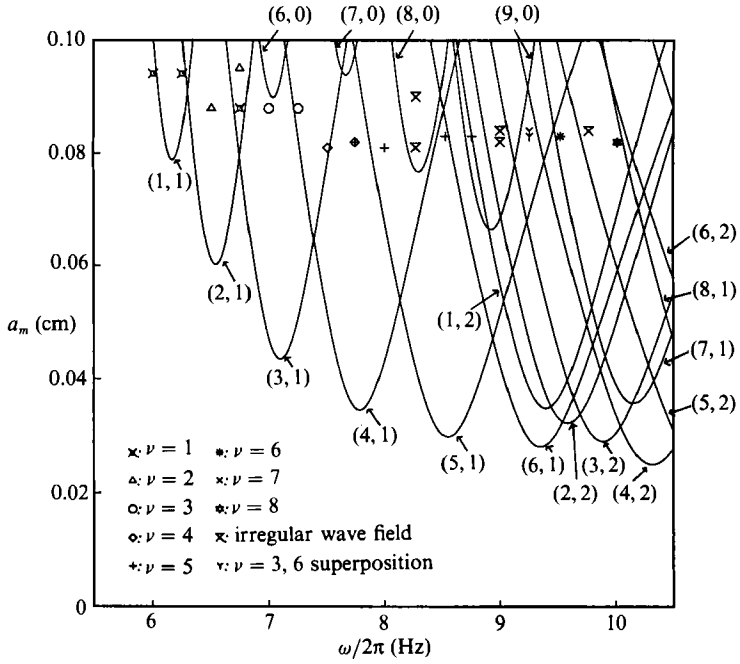

FIGURE 7. The marginal stability curves a_m *vs.* $\omega/2\pi$ as given by (C 3). The mode number (ν, m) for each curve is indicated. The (f_1, a_0) coordinates of the experiments are superimposed on these curves. Experiment 18 lies off the scale of the figure.

experiments 1, the (5, 1) mode of 8†, and the (8, 1) mode of 17†, both the axisymmetric wave and the cross-wave are stable, and either could be realized depending upon the initial conditions.

We conclude by comparing the present experimental data for standing radial cross-waves with those of Tatsuno *et al.* (1969) for progressive radial cross-waves. Figure 8(*a*, *b*) presents κr_1 versus ν for the present experimental data and those of Tatsuno *et al.* (1969). For standing radial cross-waves, the observed modes straddle the 45° line consistent with the theoretical prediction that the energy exchange coefficient Γ_1 is maximum for that mode near the turning point of Bessel's equation.† For progressive radial cross-waves, however, all of the data lie on or below the 45° line. As $r_2 \uparrow \infty$, the discrete modal spectrum determined by (1.3*b*) becomes continuous. This suggests that, without the outer cylinder to contain the weak energy input from the wavemaker, progressive radial cross-waves adjust their radial wavenumber to reduce their radiation damping by a mechanism similar to that observed by Longuet-Higgins (1967). For every experiment in figure 8(*b*) the cylinder radius, r_1 is less than (or approximately equal to for $\nu = 2$) the turning radius of Bessel's equation, ν/κ; hence, the amplitude of the progressive radial cross-wave experiences exponential decay prior to radiating its energy to infinity. A theoretical analysis of progressive radial cross-waves is in progress.

† We note that when experiment 18 is excluded, a line fitted to the experimental data in figure 8(*a*) is systematically tilted with respect to the 45° line. This behaviour is reproduced in the graph of $k_{\nu 1} r_1$ versus ν; hence, for these single-mode experiments, the $(\nu, 1)$ mode is excited.

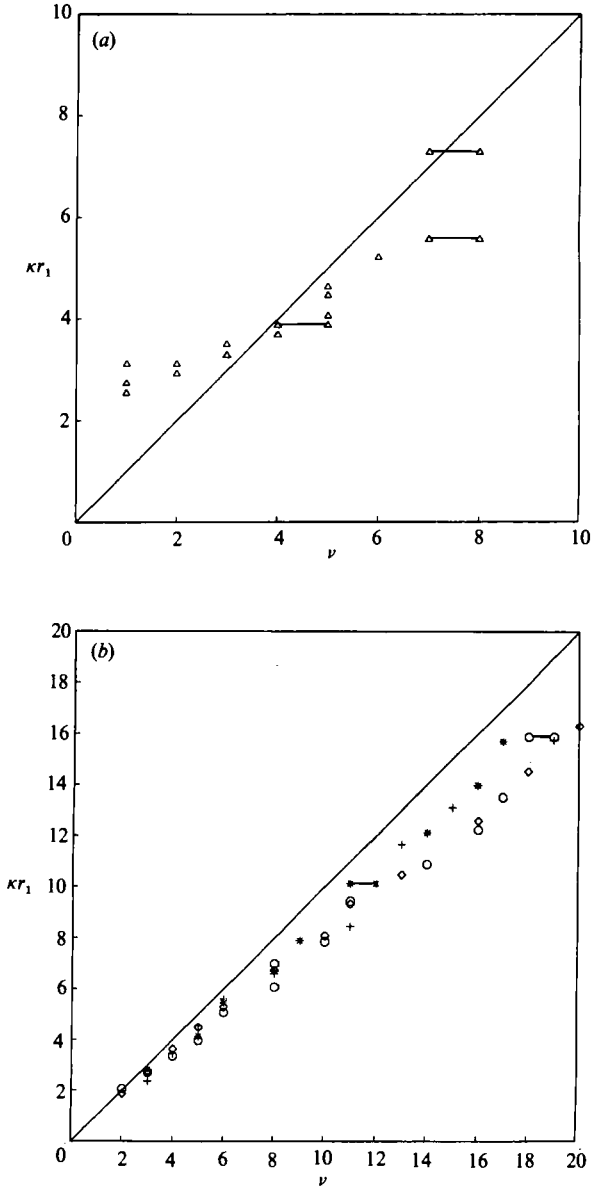

FIGURE 8. κr_1 *vs.* ν for (*a*) the present experiments on standing radial cross-waves ($r_1 = 1.89$ cm, $r_2 = 4.25$ cm) and (*b*) the experiments of Tatsuno *et al.* (1969) for progressive radial cross-waves ($r_2 \approx 29$ cm; ○, $r_1 = 1.50$ cm; ◇, $r_1 = 2.00$ cm; +, $r_1 = 2.50$ cm; *, $r_1 = 2.99$ cm). Horizontal bars indicate uncertainty in the azimuthal wavenumber ν.

REFERENCES

CILIBERTO, S. & GOLLUB, J. P. 1985 Chaotic mode competition in parametrically forced surface waves. *J. Fluid Mech.* **158**, 381–398.

GARRETT, C. J. R. 1970 On cross-waves. *J. Fluid Mech.* **41**, 837–849.

GU, X. M. & SETHNA, P. R. 1987 Resonant surface waves and chaotic phenomena. *J. Fluid Mech.* **183**, 543–565.

HAVELOCK, T. H. 1929 Forced surface waves on water. *Phil. Mag.* **8** (7), 569–576.

HENDERSON, D. M. & MILES, J. W. 1989 Single-mode Faraday waves in small containers. *J. Fluid Mech.* **213**, 95–109.

HUNT, J. N. & BADDOUR, R. E. 1980 Nonlinear standing waves bounded by cylinders. *Q. J. Appl. Maths* **33** (3), 357–371.

JONES, A. F. 1984 The generation of cross-waves in a long deep tank by parametric resonance. *J. Fluid Mech.* **138**, 53–74.

LICHTER, S. & CHEN, J. 1987 Subharmonic resonance of nonlinear cross-waves. *J. Fluid Mech.* **183**, 451–465.

LIN, J. D. & HOWARD, L. N. 1960 Non-linear standing waves in a rectangular tank due to forced oscillation. *MIT Hydrodynamics Laboratory Rep. 44.*

LONGUET-HIGGINS, M. S. 1967 On the trapping of wave energy round islands. *J. Fluid Mech.* **29**, 781–821.

LUKE, J. C. 1967 A variational principle for a fluid with a free surface. *J. Fluid Mech.* **27**, 395–397.

MACK, L. R. 1962 Periodic, finite-amplitude axisymmetric gravity waves. *J. Geophys. Res.* **67**, 829–843.

MAHONY, J. J. 1972 Cross-waves. Part 1. Theory. *J. Fluid Mech.* **55**, 229–244.

MARTIN, T. (ED.) 1932 *Faraday's Diary*, vol. 1, pp. 350–357. London: G. Bell.

MILES, J. W. 1984*a* Nonlinear Faraday resonance. *J. Fluid Mech.* **146**, 285–302; Corrigenda. *J. Fluid Mech.* **154** (1985), 535.

MILES, J. W. 1984*b* Resonantly forced motion of two quadratically coupled oscillators. *Physica* **13D**, 247–260.

MILES, J. W. 1988 Parametrically excited, standing cross-waves. *J. Fluid Mech.* **186**, 119–127.

MILES, J. W. & BECKER, J. M. 1988 Parametrically excited, progressive cross-waves. *J. Fluid Mech.* **186**, 129–146.

MILES, J. W. & HENDERSON, D. M. 1990 Parametrically forced surface waves. *Ann. Rev. Fluid Mech.* **22**, 143–165.

MILOH, T. 1984 Hamilton's principle, Lagrange's method, and ship motion theory. *J. Ship Res.* **28** (4), 229–237.

SETHNA, P. R. 1965 Vibrations of dynamical systems with quadratic nonlinearities. *J. Appl. Mech.* **32**, 576–582.

SNEDDON, I. H. 1972 *The Use of Integral Transforms.* McGraw-Hill.

TATSUNO, M., INOUE, S. & OKABE, J. 1969 Transfiguration of surface waves. *Rep. Res. Inst. Appl. Mech.* **17** (59), 195–215.

TSAI, W., YUE, D. K. P. & YIP, K. M. K. 1990 Resonantly excited regular and chaotic motions in a rectangular wavetank. *J. Fluid Mech.* **216**, 343–380.